

# Anatomical and functional dichotomy of ocular itch and pain

Cheng-Chiu Huang<sup>1,7,9</sup>, Weishan Yang<sup>1,9</sup>, Changxiong Guo<sup>1</sup>, Haowu Jiang<sup>1</sup>, Fengxian Li<sup>1,2</sup>, Maolei Xiao<sup>1</sup>, Steve Davidson<sup>3</sup>, Guang Yu<sup>4</sup>, Bo Duan<sup>5,8</sup>, Tianwen Huang<sup>5</sup>, Andrew J. W. Huang<sup>6</sup> and Qin Liu<sup>1,6\*</sup>

**Itch and pain are refractory symptoms of many ocular conditions. Ocular itch is generated mainly in the conjunctiva and is absent from the cornea. In contrast, most ocular pain arises from the cornea. However, the underlying mechanisms remain unknown. Using genetic axonal tracing approaches, we discover distinct sensory innervation patterns between the conjunctiva and cornea. Further genetic and functional analyses in rodent models show that a subset of conjunctival-selective sensory fibers marked by *MrgprA3* expression, rather than corneal sensory fibers, mediates ocular itch. Importantly, the actions of both histamine and nonhistamine pruritogens converge onto this unique subset of conjunctiva sensory fibers and enable them to play a key role in mediating itch associated with allergic conjunctivitis. This is distinct from skin itch, in which discrete populations of sensory neurons cooperate to carry itch. Finally, we provide proof of concept that selective silencing of conjunctiva itch-sensing fibers by pruritogen-mediated entry of sodium channel blocker QX-314 is a feasible therapeutic strategy to treat ocular itch in mice. Itch-sensing fibers also innervate the human conjunctiva and allow pharmacological silencing using QX-314. Our results cast new light on the neural mechanisms of ocular itch and open a new avenue for developing therapeutic strategies.**

Itch is a frequent symptom of many ocular conditions, including allergic conjunctivitis, dry eye and microbial infections<sup>1–3</sup>. Ocular itch, especially that induced by severe ocular allergy such as atopic or vernal keratoconjunctivitis, is often difficult to manage<sup>1,2,4</sup>. Compulsive rubbing or scratching itchy eyes may result in ocular infections or injuries, keratoconus and even cataracts<sup>5,6</sup>. Ocular itch mainly occurs in the conjunctiva, the mucosal membrane lining the inside of the upper and lower eyelids and covering the sclera<sup>2,4</sup>. By contrast, itch is usually absent from the cornea. It is perplexing why itch occurs in the conjunctiva rather than the cornea. Unlike the conjunctiva, the cornea lacks blood vessels and mature immune cells and is immune-privileged<sup>7,8</sup>. Because the interaction between immune cells and sensory neurons plays an essential role in many types of chronic itch<sup>9,10</sup>, the absence of immune cells may underlie the lack of itch in the cornea. However, studies have shown that compounds released from immune cells, such as histamine, are found in the tear fluids, which lubricate the cornea as well as the conjunctiva<sup>11,12</sup>; therefore, sensory fibers in the cornea can readily interact with these compounds. The mechanism underlying the conjunctival origin of ocular itch remains unclear.

Similar to but distinct from ocular itch, ocular pain represents another highly prevalent yet challenging clinical problem. Most ocular pain arises from the cornea, as it is uniquely more sensitive to mechanical and other stimuli than other parts of the eye and human body<sup>13,14</sup>. Innocuous mechanical touch or coolness, which do not evoke pain in the conjunctiva or other tissues, are often sufficient for provoking severe pain in the cornea<sup>13–17</sup>. As it is unlikely that the lack of mature immune cells in the cornea underlies either the conjunctival origin of itch or corneal pain supersensitivity, we

hypothesize that the selective origins of ocular itch and nociception are due to differences in sensory fibers innervation of the cornea and conjunctiva.

Our previous study has revealed the essential involvement of a transient receptor potential cation channel, subfamily A, member 1 (TRPA1)-mediated nonhistaminergic itch pathway in allergic ocular itch<sup>18</sup>. However, TRPA1 is expressed by both nociceptive and itch-sensing neurons<sup>19,20</sup>. It is unknown which subsets of TRPA1<sup>+</sup> sensory neurons are critical for ocular itch, and their innervation patterns in the conjunctiva and cornea are also uncertain. Recent large-scale single-cell RNA sequencing has classified three discrete populations of dorsal root ganglion (DRG) neurons with distinct repertoires of itch receptors<sup>21</sup>. The first population is defined by the expression of itch receptors for  $\beta$ -alanine (MAS-related G protein-coupled receptor member D (MrgprD)) and lysophosphatidic acid (lysophosphatidic acid receptor 3 (LPAR3) and LPAR5). This population mediates mechanical pain<sup>22</sup> and skin itch induced by  $\beta$ -alanine and cholestasis associated with elevated levels of lysophosphatidic acid<sup>21,23,24</sup>. The second population is specifically linked to skin itch. These neurons express the itch receptors *MrgprA3*, *MrgprC11* and *MrgprX1* and detect multiple pruritogens, including the itch-inducing peptides BAM8-22 and SLIGRL, the antimalaria drug chloroquine and cathepsin S<sup>21,25–29</sup>. The third population expresses neuropeptide somatostatin (SST) and itch receptors for interleukin (IL)-31, leukotriene D4 (LTD4) and serotonin, and it mediates skin itch induced by these pruritogens<sup>21,30</sup>. In addition to itch-sensing neurons, single-cell RNA sequencing also revealed two types of peptidergic nociceptive neurons and type C low-threshold mechanoreceptors (C-LTMRs) that are involved in mechanical pain

<sup>1</sup>Department of Anesthesiology and Center for the Study of Itch, Washington University School of Medicine, St. Louis, MO, USA. <sup>2</sup>Department of Anesthesiology, Zhujiang Hospital, Southern Medical University, Guangzhou, People's Republic of China. <sup>3</sup>Department of Anesthesiology and Pain Research Center, University of Cincinnati College of Medicine, Cincinnati, OH, USA. <sup>4</sup>School of Medicine and Life Sciences, Nanjing University of Chinese Medicine, Jiangsu, China. <sup>5</sup>Dana-Farber Cancer Institute and Department of Neurobiology, Harvard Medical School, Boston, MA, USA. <sup>6</sup>Department of Ophthalmology and Visual Sciences, Washington University School of Medicine, St. Louis, MO, USA. <sup>7</sup>Present address: Merck Research Laboratories, South San Francisco, CA, USA. <sup>8</sup>Present address: Department of Molecular, Cellular, and Developmental Biology, University of Michigan, Ann Arbor, MI, USA. <sup>9</sup>These authors contributed equally: Cheng-Chiu Huang, Weishan Yang. \*e-mail: [qinliu@wustl.edu](mailto:qinliu@wustl.edu)

and pleasant touch<sup>21,31</sup>. However, it is unclear whether this proposed classification of sensory fibers for DRG neurons also applies to ocular afferents and whether the selective origins of ocular itch and nociception are attributed to distinct sensory innervation patterns of the cornea and conjunctiva. To address these questions, an in-depth classification of primary sensory neurons, axonal projection and functional characterization of each population in the cornea and conjunctiva are therefore required.

## Results

**Distinct sensory innervation patterns between the cornea and conjunctiva.** Both the conjunctiva and cornea receive axonal innervation from primary sensory neurons located in the trigeminal ganglia (TG). As determined on the basis of gene expression profiles, ocular afferent neurons are heterogeneous and can be grouped into multiple subsets according to the molecular criteria used for classification of DRG neurons<sup>21</sup> (Supplementary Table 1). We found that in mice, conjunctiva and cornea as well as skin are innervated by most populations of sensory neurons, including TRPV1<sup>+</sup> heat-sensitive neurons and neuropeptide calcitonin gene-related peptide (CGRP)-expressing nociceptive neurons (Supplementary Table 2). However, low-threshold mechanosensitive C fiber neurons that express vesicular glutamate transporter 3 (VGLUT3, gene *Slc17a8*)<sup>31,32</sup> selectively innervate the whole-mount cornea but not the conjunctiva (Fig. 1a–c and Supplementary Table 2). This selective innervation pattern was further confirmed by section staining and retrograde tracing (Supplementary Fig. 1). In addition, we found that cold-sensing transient receptor potential cation channel subfamily M, member 8 (TRPM8)<sup>+</sup> sensory fibers branch extensively and terminate in the superficial layers of the corneal epithelium, but only very few TRPM8<sup>+</sup> primary afferent fibers were found in the palpebral conjunctiva (Fig. 1d–f, Supplementary Fig. 2 and Supplementary Table 2).

Finally, among the nine populations examined, two populations of primary sensory neurons were discovered that selectively innervate the conjunctiva but not the cornea (Fig. 1 and Supplementary Table 2). The first population specifically expresses MrgprD. Using an *Mrgprd*<sup>eGFP/+</sup> reporter line<sup>33</sup>, we found that MrgprD<sup>+</sup> sensory fibers innervate the conjunctiva but not the cornea (Fig. 1g–i). Dissimilar to their broad innervation in the skin, MrgprD<sup>+</sup> sensory fibers merely innervate the marginal conjunctiva (Fig. 1g,h). This region contacts with the ocular surface during blinking and is termed the lid wiper<sup>34</sup>.

The second population expresses MrgprA3. Using *Mrgpra3*<sup>GFP-cre</sup>; *Rosa26*<sup>tdTomato/+</sup> (*Mrgpra3*<sup>tdTomato</sup>) mice<sup>26</sup>, we found that MrgprA3<sup>+</sup> sensory fibers selectively innervate the conjunctiva but are completely absent from the cornea and tested mucosal tissues, including nasal and oral mucosa, rectum and vagina (Fig. 1j–o). MrgprA3<sup>+</sup> sensory terminals are particularly enriched in the conjunctiva close to the medial and lateral canthi (corners of the eye), regions that are most sensitive to itch. This selective innervation pattern was further confirmed by retrograde tracing (Supplementary Fig. 3), suggesting a role for MrgprA3<sup>+</sup> sensory fibers in ocular itch. The other population of itch-related sensory neurons that express SST is completely absent from both the conjunctiva and cornea (Fig. 1p–r), despite their dense innervation in the skin (Fig. 1r). Distinct sensory innervation patterns of the cornea and conjunctiva were further confirmed by single-cell RT-PCR (Fig. 1s and Supplementary Table 1).

**A subset of conjunctival-selective sensory fibers mediates ocular itch.** To test the hypothesis that ocular itch is mediated by conjunctiva-selective sensory fibers, we studied the function of corneal- or conjunctiva-selective sensory neurons in ocular itch. We first examined the involvement of corneal TRPM8<sup>+</sup> sensory fibers in ocular itch. Exposing mouse eyes to cold air flow (13 °C) or menthol (an organic compound from peppermint that selectively

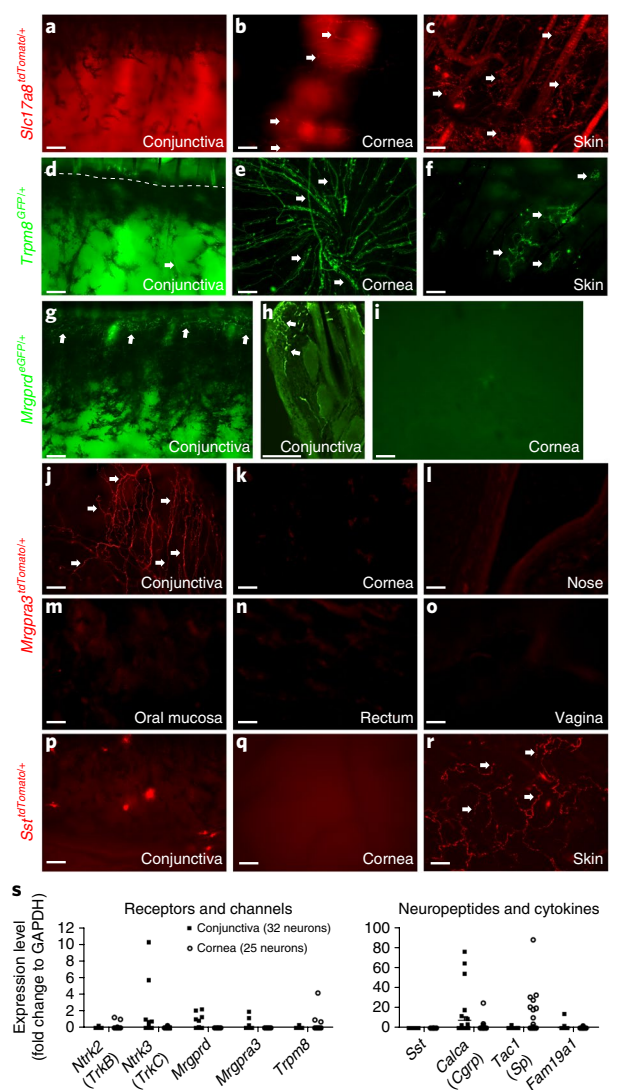


**Fig. 1 | There are distinct sensory innervation patterns between the cornea and conjunctiva.** **a–c**, Representative images showing the innervation patterns of type C low-threshold mechanoreceptors (C-LTMRs) that express VGLUT3 in the whole-mount conjunctiva (**a**), cornea (**b**) and skin (**c**) from *Slc17a8*<sup>cre/+</sup>; *Rosa26*<sup>tdTomato/+</sup> (*Slc17a8*<sup>tdTomato/+</sup>) mice. Arrows indicate *SLC17A8*-expressing fibers. **d–f**, Representative images showing the innervation patterns of cold-sensitive C fibers that express TRPM8 in the whole-mount conjunctiva (**d**), cornea (**e**) and skin (**f**) from *Trpm8*<sup>GFP/+</sup> mice. Arrows indicate TRPM8<sup>+</sup> fibers. The dashed line in **d** indicates the boundary between the conjunctiva and eyelid skin. **g–i**, Representative images showing the innervation patterns of MrgprD<sup>+</sup> sensory fibers in the conjunctiva (whole-mount (**g**); section (**h**)) and whole-mount cornea (**i**) from *Mrgprd*<sup>GFP/+</sup> mice. Arrows indicate MrgprD<sup>+</sup> fibers. **j–o**, Representative images showing the innervation patterns of MrgprA3<sup>+</sup> sensory fibers in the whole-mount palpebral conjunctiva (**j**), cornea (**k**), nose (**l**), oral mucosa (**m**), rectum (**n**) and vagina (**o**) from *Mrgpra3*<sup>cre/+</sup>; *Rosa26*<sup>tdTomato/+</sup> (*Mrgpra3*<sup>tdTomato/+</sup>) mice. **p–r**, Representative images showing the innervation patterns of somatostatin (SST)-expressing sensory fibers in the whole-mount conjunctiva (**p**), cornea (**q**) and skin (**r**) from *Sst*<sup>cre/+</sup>; *Rosa26*<sup>tdTomato/+</sup> (*Sst*<sup>tdTomato/+</sup>) mice. Arrows indicate SST<sup>+</sup> fibers. All images shown are representative of three independent experiments using tissues from at least three different mice. Scale bars, 100 μm. **s**, Results from single-cell qRT-PCR of trigeminal ganglion neurons retrogradely labeled from the cornea or conjunctiva. Each dot represents one sensory neuron. One data point of *Tac1* (995.48 in the cornea group) is outside the axis limit. All data are expressed as mean ± s.e.m.

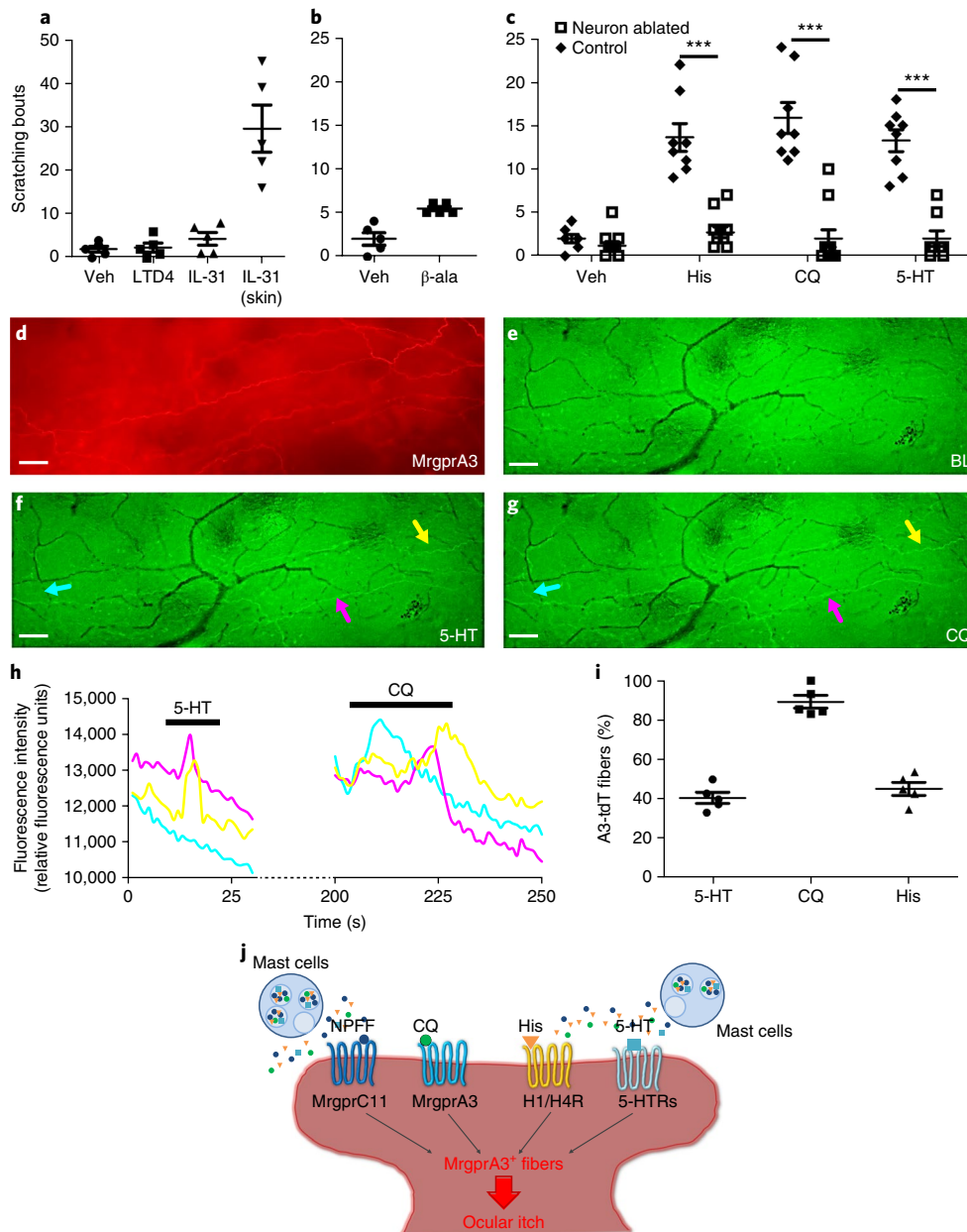


**Fig. 2 | Conjunctival *MrgprA3*<sup>+</sup> sensory neurons mediate acute ocular itch.** **a**, Scratching response induced by conjunctival application of leukotriene D<sub>4</sub> (LTD<sub>4</sub>, 10 pmol in 2.5  $\mu$ l) or IL-31 (25 pmol in 2.5  $\mu$ l), nape intradermal injection of IL-31 (100 pmol in 50  $\mu$ l) or saline vehicle (Veh) in WT mice ( $n=5$  per group). **b**, Ocular scratching responses evoked by saline vehicle and  $\beta$ -alanine ( $\beta$ -ala; 500 nmol in 2.5  $\mu$ l) in WT mice ( $n=5$  per group). **c**, Ocular scratching responses induced by histamine (His; 250 nmol in 2.5  $\mu$ l), chloroquine (CQ; 24 nmol in 2.5  $\mu$ l), serotonin (5-HT; 940 pmol in 2.5  $\mu$ l) in *MrgprA3*<sup>+</sup> neuron-ablated ( $n=11$ /group for histamine and chloroquine assays, and  $n=9$  for serotonin assay) and WT mice ( $n=8$ /group). Statistical analysis by two tailed Student's *t*-test (histamine,  $***P=0.0001$ ; chloroquine,  $***P=0.000001$ ; serotonin,  $***P=0.000007$ ). **d**, Representative images showing *MrgprA3*<sup>+</sup> fibers (labeled by tdTomato, red) in the conjunctiva from *Pirt*<sup>GCaMP3/+</sup>; *MrgprA3*<sup>tdTomato</sup> mice ( $n=3$ ). **e–g**, Representative images showing the fluorescence changes of GCaMP3 in the conjunctival sensory fibers at baseline (BL; **e**) or upon stimulation with serotonin (100  $\mu$ M; **f**) and chloroquine (2 mM; **g**). Scale bars, 50  $\mu$ m. **h**, Ca<sup>2+</sup> transients of representative *MrgprA3*<sup>+</sup> sensory fibers (highlighted by the corresponding colored arrows in **f**, **g**). **i**, Percentages of *MrgprA3*-tdTomato-expressing sensory fibers that were activated by different pruritogens (5-HT,  $40.7 \pm 2.5\%$ ; CQ,  $89.4 \pm 2.8\%$ ; His,  $45.3 \pm 2.9\%$ ). Each dot represents a conjunctiva explant from a *Pirt*<sup>GCaMP3/+</sup>; *MrgprA3*<sup>tdTomato</sup> mouse ( $n=5$  conjunctivae from 3 mice per group). All data are expressed as mean  $\pm$  s.e.m. **j**, Diagram showing the actions of both histamine and nonhistamine pruritogens converging onto *MrgprA3*<sup>+</sup> sensory fibers to induce ocular itch.

activates TRPM8) provokes pain-related blinking and eye-closing responses, rather than itch-related scratching behavior, in wild-type (WT) mice. TRPM8-deficiency entirely abolished pain responses to cold stimuli (Supplementary Fig. 4), indicating that TRPM8 mediates corneal cold supersensitivity.

To further study the function of conjunctival-selective sensory fibers in ocular sensation, we typically applied itch- or pain-inducing

chemicals to the lower conjunctival sac in mice<sup>18</sup>. We discovered that IL-31 and LTD<sub>4</sub>, two immune factors that selectively activate SST<sup>+</sup> sensory neurons in the skin<sup>21</sup>, failed to generate ocular itch-related scratching or pain-related wiping behavior in mice (Fig. 2a), corroborating the absence of SST<sup>+</sup> sensory fibers in the conjunctiva. As a control, IL-31 evokes remarkable itch in the skin (Fig. 2a), as reported previously<sup>21,30,35</sup>. Next, we examined the role of *MrgprD*<sup>+</sup>

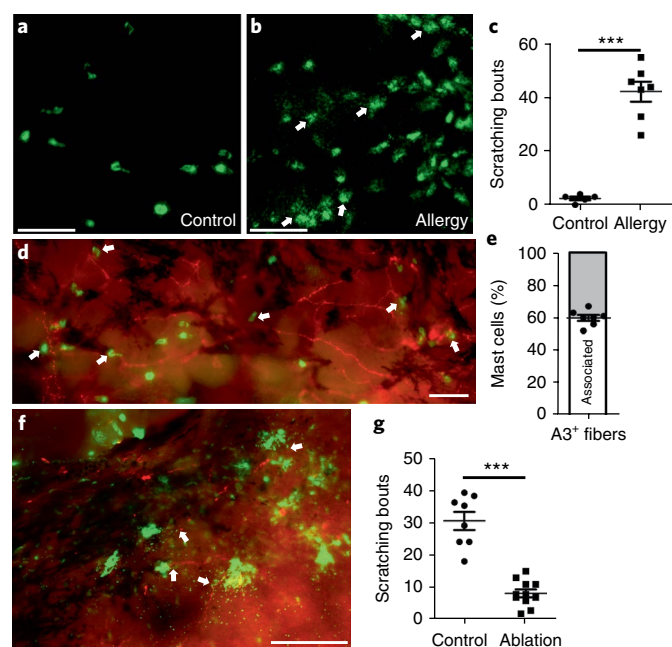


**Fig. 3 | MrgprA3<sup>+</sup> sensory neurons are required for mast cell-dependent allergic ocular itch.** **a, b**, Representative images of mast cells (stained with FITC-avidin, green) in the whole-mount conjunctivae of nonimmunized (**a**) and ovalbumin-immunized mice (**b**). Arrows indicate the granules released from mast cell bodies upon challenging with the allergen ovalbumin. **c**, Ocular scratching responses evoked by topical conjunctival application of allergen ovalbumin in nonallergic control mice ( $n=5$ ) and allergic mice ( $n=7$ ). Statistical analysis by two tailed Student's  $t$ -test ( $***P=0.00003$ ). **d**, Representative image of the whole-mount conjunctiva from *Mrgpra3<sup>tdTomato</sup>* mice. Arrows indicate avidin-stained mast cells. **e**, The proportion of mast cells closely associated with MrgprA3<sup>+</sup> sensory fibers ( $n=7$  conjunctival explants). **f**, Representative image showing the interaction between released granules (green) and MrgprA3<sup>+</sup> sensory fibers (red) in the conjunctiva upon allergen challenge, as indicated by arrows. All images shown are representatives of three independent experiments using tissues from at least three different mice. Scale bars, 50  $\mu\text{m}$ . **g**, Ocular scratching responses induced by mast cell-dependent ocular allergy in MrgprA3<sup>+</sup> neuron-ablated mice ( $n=11$ ) and control *Rosa26<sup>HBEGR/+</sup>* mice ( $n=8$ ). Statistical analysis by two tailed Student's  $t$ -test ( $***P=0.0000003$ ). All data are expressed as mean  $\pm$  s.e.m.

neurons in ocular sensation. Using  $\beta$ -alanine (a MrgprD agonist) as a stimulant, we found that activation of MrgprD<sup>+</sup> neurons only evoked minimal ocular scratching (Fig. 2b), providing evidence against an important role for these neurons in ocular itch. The fact that the innervation of MrgprD<sup>+</sup> neurons is restricted to the lid wiper region of the conjunctiva (Fig. 1g,h) supports the notion that these neurons sense eye blinking and tearing rather than itch.

Finally, we tested the role of MrgprA3<sup>+</sup> neurons in ocular itch. We found that ablation of MrgprA3<sup>+</sup> sensory neurons (Supplementary Fig. 5) significantly reduces ocular itch induced by an array of itch-inducing molecules. Chloroquine, the agonist for MrgprA3<sup>25</sup>, elicits significant ocular itch in WT mice, but not in MrgprA3<sup>+</sup> neuron-ablated mice (Fig. 2c). In addition, neuropeptide FF (NPFF), an agonist for itch receptor MrgprC11<sup>36</sup>, also induces ocular itch in an Mrgpr-dependent manner. Ocular itch induced by histamine and serotonin is abolished in MrgprA3<sup>+</sup> neuron-ablated mice as well (Fig. 2c). This result is entirely unexpected, as histamine and serotonin can activate MrgprA3-independent itch-sensing fibers in the skin, and ablation of MrgprA3<sup>+</sup> neurons cannot completely abolish the skin itch induced by these pruritogens<sup>21,26,30,37</sup>. Our results

demonstrate that the underlying mechanisms involved in ocular itch and skin itch are different and that MrgprA3<sup>+</sup> sensory neurons play a more predominant role in ocular itch than in skin itch.

We further characterized the physiological properties of MrgprA3<sup>+</sup> neurons that innervate the conjunctiva by crossing *MrgprA3<sup>tdTomato</sup>* mice with *Pirt<sup>GCaMP3/+</sup>* mice expressing the calcium indicator GCaMP3 in primary sensory neurons<sup>38</sup>. The resulting *Pirt<sup>GCaMP3/+</sup>; Mrgpra3<sup>tdTomato</sup>* mouse line allows ex vivo imaging of calcium mobilization in MrgprA3<sup>+</sup> sensory fibers (labeled by tdTomato) in response to pruritogens applied onto the conjunctiva (Fig. 2d–i and Supplementary Fig. 6). Indeed, we discovered that MrgprA3<sup>+</sup> fibers respond to a range of itch-inducing chemicals with an increased concentration of intracellular Ca<sup>2+</sup> ([Ca<sup>2+</sup>]<sub>i</sub>), including histamine, serotonin, chloroquine and NPFF (Fig. 2d–i and Supplementary Fig. 6), correlating well with our in vivo behavioral results. Notably, MrgprA3<sup>+</sup> sensory neurons innervating body skin failed to respond to serotonin (Supplementary Fig. 7). Instead, MrgprA3-independent SST<sup>+</sup> sensory neurons mediate serotonin-induced itch in the skin<sup>30</sup>. Our results thus support that MrgprA3<sup>+</sup> sensory fibers in the conjunctiva incorporate a partial function of SST<sup>+</sup> sensory neurons and are different from those innervating the skin (Fig. 2j), providing a molecular basis for the predominant role of MrgprA3<sup>+</sup> sensory neurons in ocular itch. Interestingly, histamine, serotonin and NPFF have been reported to be secreted from mast cells<sup>36,39,40</sup>, suggesting that conjunctival MrgprA3<sup>+</sup> sensory neurons might detect itch mediators from mast cells in allergy and mediate ocular itch associated with allergic conjunctivitis (Fig. 2j). Indeed, conjunctival allergen challenge elicited significant degranulation of mast cells and scratching behavior directed to the treated eye in immunized WT mice (Fig. 3a–c). Notably, we found that mast cells are closely associated with MrgprA3<sup>+</sup> sensory fibers in the conjunctiva (Fig. 3d,e). Upon degranulation of a mast cell, granules directly interact with MrgprA3<sup>+</sup> sensory fibers (Fig. 3f). Ablation of MrgprA3<sup>+</sup> neurons significantly reduced allergic ocular itch (Fig. 3g), indicating that MrgprA3<sup>+</sup> sensory fibers are the principal itch-sensing fibers for inflammatory mediators released by conjunctival mast cells in this allergic conjunctivitis model.

**The central neural circuit for ocular itch.** Studies have revealed distinct central representations for sensory fibers innervating either the conjunctiva or cornea<sup>41</sup>. However, it is unclear whether this anatomical difference underlies the conjunctival origin of ocular itch and corneal insensitivity to itch. Neuromedin B (NMB) is a bombesin-related peptide and is highly expressed in small-diameter sensory neurons, including MrgprA3<sup>+</sup> neurons<sup>42,43</sup>. Its function in pain and itch, however, remains controversial<sup>42,44</sup>. Interestingly, we found that NMB is highly expressed in the sensory neurons innervating the conjunctiva but not the cornea (Fig. 4a–g). Importantly, *Nmb*-null mice display significantly reduced ocular itch (Fig. 4i) but normal responses to ocular pain, suggesting that NMB is required for transmission of the itch signal from ocular afferent fibers. Furthermore, NMBR, the receptor for NMB, is found in the central projection area of sensory fibers innervating the conjunctiva as well as the neighboring area that may receive sensory inputs from the skin sensory fibers (such as those from the eyelid skin) (Fig. 4j). However, NMBR is completely absent from the central projection area of the cornea (Fig. 4h). Similar to NMB deficiency, deletion of NMBR leads to a significant reduction in ocular itch (Fig. 4i). These results indicate that NMB–NMBR signaling is required for conjunctival itch transmission, providing a new central mechanism explaining why the cornea is not ‘itch’ sensitive.

**Development of a new therapeutic strategy for allergic ocular itch.** To test whether selective silencing of MrgprA3<sup>+</sup> sensory fibers using pharmacological approaches is a feasible therapeutic strategy to provide sustained relief of ocular itch, we adopted an approach

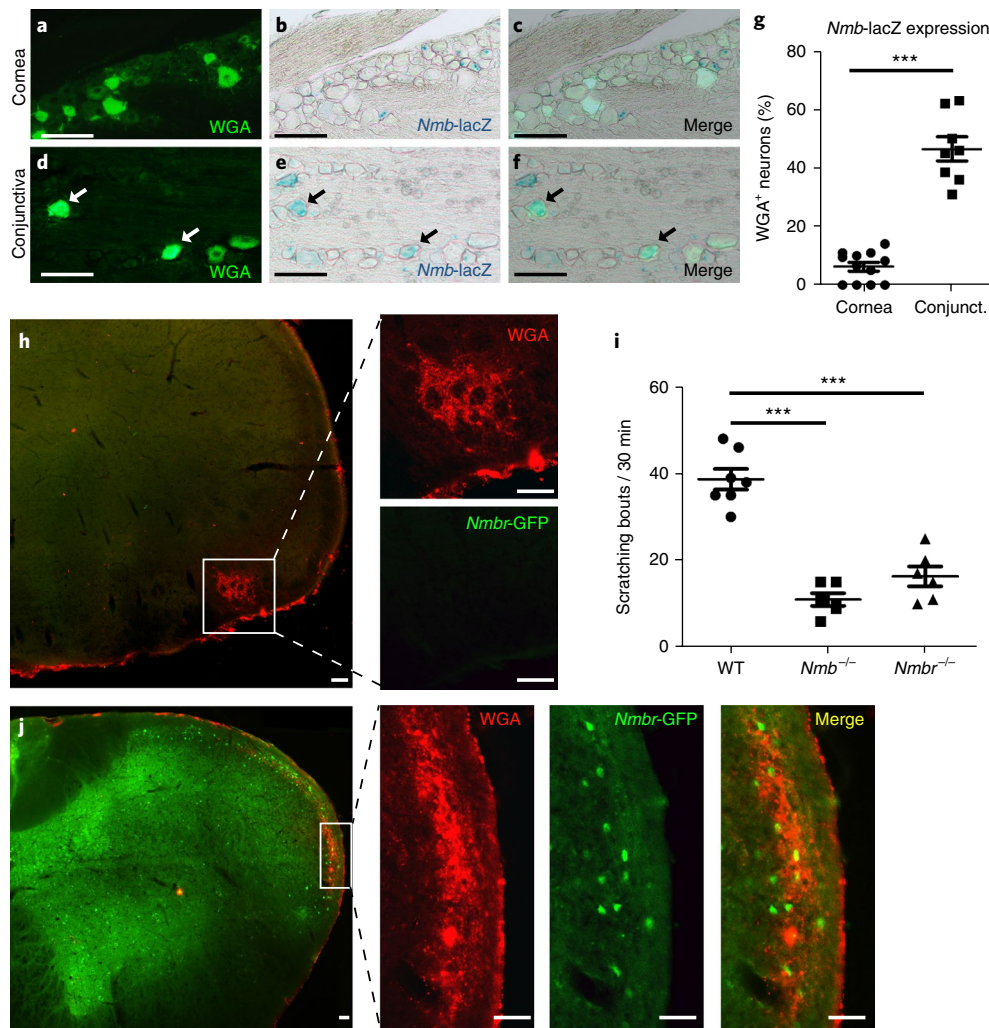


**Fig. 4 | Central NMB-NMBR signaling is required for conjunctival itch transmission.** **a–g.** Representative images showing X-gal staining of the *Nmb*-lacZ reporter in sections containing sensory neurons retrogradely labeled by wheat germ agglutinin (WGA) conjugated with Alexa Fluor 488 (WGA-488) from the conjunctiva or cornea of *Nmb<sup>tm1.1(KOMP)Vlgg</sup>* mice (**a–f**) and quantification (**g**). Each point in **g** represents data from one section image of trigeminal ganglia ( $n=6$  trigeminal ganglia from 3 mice per group). Statistical analysis by two tailed Student's *t*-test ( $***P=0.000008$ ). **h, j.** Representative images showing the absence or presence of *Nmbr*-GFP in the central projection area of corneal (**h**) or conjunctival (**j**) afferent neurons. Scale bars, 50  $\mu$ m. **i.** Ocular scratching responses evoked by ocular allergy in *Nmb<sup>-/-</sup>* mice ( $n=5$ ), *Nmbr<sup>-/-</sup>* mice ( $n=6$ ) and WT (control) mice ( $n=7$ ). Statistical analysis by one-way ANOVA followed by two tailed Student's *t*-test (*Nmb<sup>-/-</sup>* versus WT,  $***P=0.000002$ ; *Nmbr<sup>-/-</sup>* versus WT,  $***P=0.00004$ ). All data are expressed as mean  $\pm$  s.e.m.

of reversibly silencing MrgprA3<sup>+</sup> fibers by targeted delivery of a charged sodium-channel blocker, QX-314. QX-314 is membrane-impermeable and can only enter the cell through large pores of ion channels opened upon neuronal excitation<sup>45,46</sup>. Because TRPA1 is the downstream transduction channel of MrgprA3 (ref. <sup>20</sup>, QX-314 would be able to permeate into MrgprA3<sup>+</sup> neurons via the opening of TRPA1 upon chloroquine challenge (Supplementary Fig. 8a). Indeed, using *Mrgpra3<sup>tdTomato</sup>* mice, we confirmed that chloroquine-mediated activation of TRPA1 channels allows sufficient QX-314 uptake to suppress voltage-dependent inward sodium currents in MrgprA3<sup>+</sup> neurons (Supplementary Fig. 8b–e). This reduction in sodium currents was sufficient to suppress the generation of action potentials in MrgprA3<sup>+</sup> neurons (Fig. 5a–d). Furthermore, application of a low concentration of chloroquine (4 mM; Supplementary Fig. 9) and QX-314 (1%, 2  $\mu$ l) onto the conjunctiva effectively suppressed the subsequent ocular itch induced by chloroquine (12 mM) applied 30 min later (Fig. 5e), suggesting that conjunctival MrgprA3<sup>+</sup> sensory fibers can be silenced *in vivo*. Importantly, this pretreatment of QX-314 with chloroquine remarkably alleviated

allergic ocular itch in mice for more than 24 h, and its efficacy diminished through the next 24 h (Fig. 5f). In contrast, the anti-itch effects of an antihistamine, pheniramine, diminished within 1 h (Fig. 5g). Thus, selective silencing of MrgprA3<sup>+</sup> sensory fibers provides more potent and sustained relief of allergic ocular itch than the conventional antihistamine (Fig. 5h).

We next examined the effects of silencing itch-sensing fibers on migration and infiltration and activation of immune cells (particularly mast cells). Allergen challenge induces extensive mast cell accumulation and degranulation (Fig. 5i–k). Silencing of MrgprA3<sup>+</sup> sensory fibers effectively diminished mast cell accumulation (Fig. 5i–j) but did not reduce mast cell degranulation. In contrast, pheniramine did not affect mast cell accumulation or immune cell infiltration (Fig. 5i–k). To investigate the mechanisms underlying the immune regulatory effect of silencing itch-sensing afferent fibers, we tested whether MrgprA3<sup>+</sup> sensory neurons produce neuropeptides capable of attracting immune cells. Although substance P can directly activate mast cells<sup>47,48</sup>, it was not expressed in MrgprA3<sup>+</sup> neurons (Supplementary Fig. 10), consistent with our single-cell

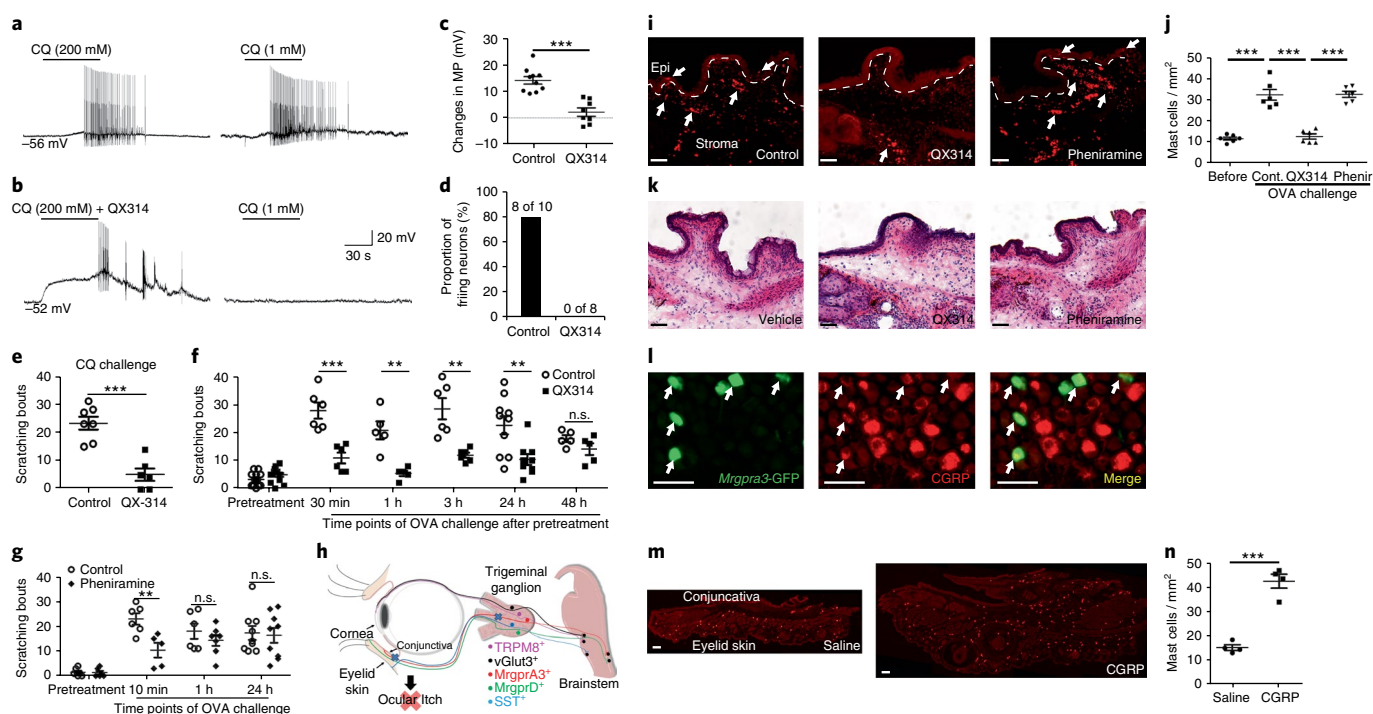


**Fig. 5 | Pharmacological silencing of *MrgprA3*<sup>+</sup> neurons reduces both acute and allergic ocular itch.** **a**, Representative traces of action potentials elicited by repeated chloroquine application were chosen from ten recorded *MrgprA3*<sup>+</sup> sensory neurons in the control group. **b**, Representative traces of action potentials induced by application of QX-314 plus chloroquine and subsequent chloroquine alone were chosen from eight recorded *MrgprA3*<sup>+</sup> neurons in the QX-314 group. **c**, Changes in the membrane potential (MP) in control ( $n=10$ ) and QX-314 ( $n=8$ ) groups. Statistical analysis by two-tailed Student's  $t$ -test ( $***P=0.00003$ ). **d**, The proportion of firing neurons in control and QX-314 groups. **e**, Ocular scratching responses induced by conjunctival application of CQ (12 mM) after pretreatments of 4 mM CQ and 1% QX-314 (QX-314 group,  $n=6$ ) compared with the control group pretreated with 4 mM CQ alone ( $n=7$ ). Statistical analysis by two-tailed Student's  $t$ -test ( $***P=0.0001$ ). **f**, Allergen ovalbumin (OVA)-induced ocular scratching responses at different time points after pretreatment of 4 mM CQ and 1% QX-314 compared with controls pretreated with 4 mM CQ alone ( $n=14$  (pretreatment), 6 (30 min), 5 (1 h), 6 (3 h), 10 and 9 (24 h), 5 (48 h) mice). Statistical analysis by two-tailed Student's  $t$ -test (30 min,  $***P=0.0006$ ; 1 h,  $**P=0.007$ ; 3 h,  $**P=0.006$ ; 24 h,  $**P=0.006$ ). **g**, Allergen ovalbumin-induced ocular scratching responses at different time points after pretreatment of pheniramine (0.4%, 2  $\mu$ l) or vehicle control ( $n=6$  (pretreatment), 6 and 5 (10 min), 6 and 7 (1 h), 9 (24 h) mice). Statistical analysis by two-tailed Student's  $t$ -test ( $**P=0.007$ ). **h**, A diagram summarizing the predominant role of *MrgprA3*<sup>+</sup> sensory neurons in ocular itch. **i**, Representative images of vehicle-treated (control), QX-314-treated and pheniramine-treated conjunctivae under allergic conjunctivitis. The dashed lines indicate the boundary between the epithelium and stroma of the conjunctivae; white arrows indicate the mast cells. **j**, Quantitative analysis of mast cell number after different treatments (each dot represents a conjunctiva explant;  $n=6$  conjunctivae from 3 mice per group). Statistical analysis by one-way ANOVA followed by two-tailed Student's  $t$ -test (before versus control (cont.),  $***P=0.0003$ ; cont. versus QX314,  $***P=0.00004$ ; QX314 versus pheniramine,  $***P=0.000001$ ). **k**, Representative H&E staining showing inflammatory cell infiltration in vehicle, QX-314 and pheniramine-treated allergic conjunctiva after allergen (ovalbumin) challenges. **l**, Representative images showing the expression of neuropeptide CGRP (red) in *MrgprA3*<sup>+</sup> sensory neurons (green), as indicated by arrows. **m**, Representative images showing mast cells in the conjunctivae after treatments of CGRP (0.5 nmol in 2.5  $\mu$ l) or saline. All images shown are representatives of three biologically independent mice. Scale bars in all images, 50  $\mu$ m. **n**, Quantitative analysis of mast cell number after CGRP treatments (each dot represents a conjunctiva explant;  $n=4$  conjunctivae from 3 mice per group). Statistical analysis by two-tailed Student's  $t$ -test ( $***P=0.0001$ ). All data are expressed as mean  $\pm$  s.e.m.

qRT-PCR results (Supplementary Table 1) and previous findings<sup>26</sup>. In contrast, we detected the expression of neuropeptide CGRP in *MrgprA3*<sup>+</sup> neurons (Fig. 5l). The administration of CGRP peptide into the mouse conjunctiva sac unexpectedly recruited more mast cells but did not cause mast cell degranulation or itch (Fig. 6m,n).

**Conserved innervation pattern and function of itch-sensing afferent fibers in human conjunctiva.** Our finding of mouse *MrgprA3*<sup>+</sup> sensory fibers in ocular itch raises the question of whether human *Mrgpr* (*hMrgpr*)-expressing sensory fibers play a similar role in itch perception. Among all the human *Mrgprs*, *hMrgprX1* is sensitive to chloroquine and corresponds to mouse *MrgprA3* (ref. 25). Hence, we examined the innervation pattern of *hMrgprX1*<sup>+</sup> sensory fibers in the eye using a newly generated anti-*hMrgprX1* antibody. The antibody selectively stained sensory neurons of *MRGPRX1*; *Mrgpr-cluster* $\Delta^{-/-}$  mice, in which *hMrgprX1*, instead of mouse

*Mrgpr*, is expressed in mouse sensory neurons, but not those from *Mrgpr-cluster* $\Delta^{-/-}$  mice (Fig. 6a,b), indicating that the antibody specifically recognizes *hMrgprX1*. Using this antibody, we found that *hMrgprX1*<sup>+</sup> sensory fibers selectively innervate the conjunctiva but not the cornea of human eyes (Fig. 6c,d), correlating well with the innervation pattern of itch-sensing fibers in mice.

To determine whether the activation of *hMrgprX1* allows the entry of QX-314 via TRPA1 channels, we examined whether TRPA1 is the downstream transduction channel of *hMrgprX1* in TG sensory neurons from *MRGPRX1*; *Mrgpr-cluster* $\Delta^{-/-}$  mice. We found that the chloroquine triggered a train of action potentials in *hMrgprX1*-expressing sensory neurons (identified by calcium imaging; Fig. 6e,f). Importantly, pretreatment with TRPA1 antagonist HC030031 effectively suppressed the neuronal discharge in response to chloroquine (Fig. 6e,f), indicating that TRPA1 is the downstream transduction channel of *hMrgprX1* and is required for

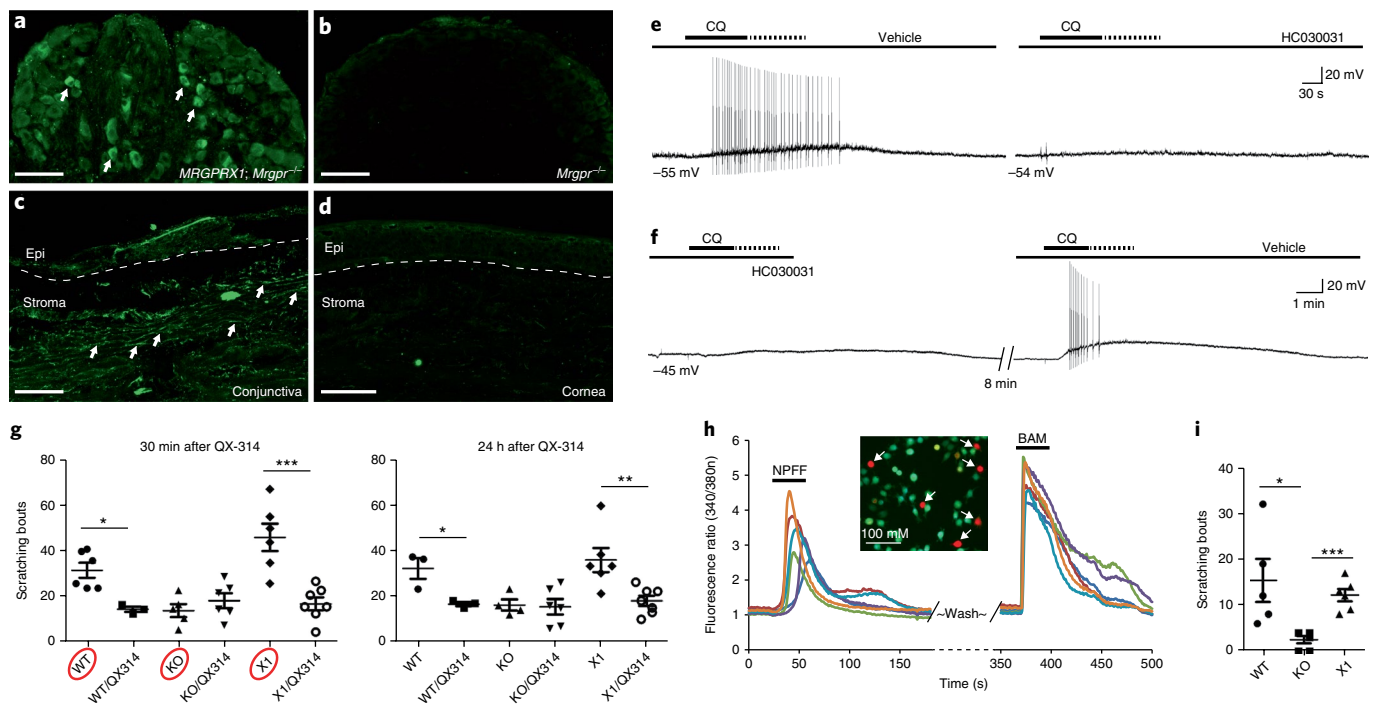


**Fig. 6 | *MrgprX1*<sup>+</sup> sensory afferents selectively innervate human conjunctiva and mediate itch in a humanized mouse model. **a, b**, Representative images showing immunofluorescent staining of sensory neurons from *MRGPRX1*; *Mrgpr-clusterΔ*<sup>-/-</sup> and *Mrgpr-clusterΔ*<sup>-/-</sup> mice using a newly generated antibody against hMrgprX1. Arrows indicate sensory neurons labeled by the anti-hMrgprX1 antibody. **c, d**, Representative images showing immunofluorescent staining of human conjunctiva and cornea using anti-hMrgprX1 antibody. The arrows indicate sensory fibers labeled by anti-hMrgprX1 antibody. The dashed lines indicate the boundary between the epithelium (Epi) and stroma. Images shown are representative of three biologically independent samples. Scale bars, 100 μm. **e, f**, Representative traces of action potentials elicited by chloroquine (1 mM) stimulation in hMrgprX1-expressing sensory neurons (as determined by calcium imaging using BAM8-22; *n* = 5). The recorded neurons received pretreatments of vehicle control and 100 μM HC030031 (100 μM) (**e**) or that in reverse order (**f**). **g**, Scratching responses induced by conjunctiva challenge with allergen ovalbumin in immunized WT, *Mrgpr-clusterΔ*<sup>-/-</sup> and *MRGPRX1*; *Mrgpr-clusterΔ*<sup>-/-</sup> mice with or without pretreatments of 1% QX-314 with 4 mM chloroquine (30 min; *n* = 6 and 3 (WT group), 5 and 6 (KO group), 6 and 7 (X1 group); 24 h, *n* = 3 and 3 (WT group), 4 and 6 (KO group), 6 and 7 (X1 group)). Statistical analysis by two-tailed Student's *t*-test (WT versus WT/QX314: 30 min \**P* = 0.011, 24 h \**P* = 0.03; X1 versus X1/QX314: 30 min \*\*\**P* = 0.0007, 24 h \*\**P* = 0.007). **h**, Representative calcium transients of hMrgprX1-expressing heterologous cells in response to NPFF (6 μM) and BAM8-22 (2 μM). In the inset, arrows indicate BAM8-22-responsive hMrgprX1-expressing cells that were activated by NPFF. **i**, Scratching responses induced by conjunctival application of NPFF (2.5 nmol in 2.5 μl) in WT (*n* = 5), *Mrgpr-clusterΔ*<sup>-/-</sup> (*n* = 6) and *MRGPRX1*; *Mrgpr-clusterΔ*<sup>-/-</sup> mice (*n* = 6). Statistical analysis by one-way ANOVA (*P* = 0.0082) followed by two-tailed Student's *t*-test (WT versus KO, \**P* = 0.016; KO versus X1, \*\*\**P* = 0.0001). All data are expressed as mean ± s.e.m.**

the depolarization of hMrgprX1<sup>+</sup> neurons. We further examined the feasibility of selectively silencing hMrgprX1<sup>+</sup> sensory fibers using QX-314 for itch treatment. We found that neuronal silencing is effective in alleviating allergic ocular itch in *MRGPRX1*; *Mrgpr-clusterΔ*<sup>-/-</sup> mice (Fig. 6g). The anti-itch effect lasts for at least 24 h in this humanized mouse model (Fig. 6g). Importantly, QX-314-mediated neuronal silencing is ineffective in *Mrgpr-clusterΔ*<sup>-/-</sup> mice (Fig. 6g) because of a lack of Mrgprs required for chloroquine-mediated entry of QX-314 into ocular itch fibers, demonstrating the specificity of this neuronal silencing approach. Notably, deficiency in Mrgprs considerably reduces ocular itch in *Mrgpr-clusterΔ*<sup>-/-</sup> mice, suggesting an indispensable role for Mrgprs in mediating ocular itch. This itch defect can be entirely rescued by the expression of hMrgprX1 in *MRGPRX1*; *Mrgpr-clusterΔ*<sup>-/-</sup> mice (Fig. 6g), indicating that hMrgprX1 mediates ocular itch and provides a new drug target for ocular itch.

To understand the mechanism through which hMrgprX1 mediates allergic ocular itch, we examined whether hMrgprX1 can be activated by itch mediators released from mast cells in allergy. Our previous study shows that NPFF can be released from mast cells and activate sensory neurons via mouse MrgprC11 (ref. 36). Here, we found that NPFF also activates hMrgprX1, as revealed by calcium imaging (Fig. 6h). Importantly, NPFF induces significant ocular

itch in a manner dependent on mouse Mrgpr or hMrgprX1 (Fig. 6i). These data suggest that hMrgprX1 is capable of detecting itch mediators (such as NPFF) released from mast cells, providing one of the mechanisms through which hMrgprX1 mediates allergic ocular itch. Together, our results indicate that hMrgprX1 is a principal itch receptor for ocular itch and hence a promising drug target for itch management.

## Discussion

The findings of conjunctiva- and cornea-selective sensory innervations substantially advance our understanding of the neural basis underlying the dichotomy of ocular itch and pain. The conjunctiva plays an important role in immune surveillance and helps prevent the entrance of microbes into the eye. The selective projection of itch-sensing fibers to the conjunctiva enables the peripheral sensory system to monitor immune homeostasis and initiate an alarm when the immune system is dysregulated. Indeed, itch is closely associated with many types of immune disorders in the conjunctiva, including allergy, infection and inflammation. By contrast, to maintain its transparency for refracting light and focusing our vision, the cornea lacks blood vessels and is immune privileged<sup>7,8</sup>. Hence, the immune surveillance function of itch-sensing fibers is not required for the cornea. Moreover,

the cornea is very fragile and easily damaged. Studies have shown that chronic eye rubbing causes corneal thinning and keratoconus, a condition in which the shape of the cornea becomes irregular or conical. As a protective mechanism, the cornea is densely innervated by subsets of primary sensory fibers and generates pain in response to normally innocuous stimuli. Our finding of the lack of itch-sensing fibers and the NMB–NMBR-dependent itch pathway in the cornea offers an extra protective mechanism to prevent the cornea from becoming itchy. This newly described mechanism, combined with corneal supersensitivity, effectively protects the cornea from mechanical damages caused by scratching or rubbing.

The finding of conjunctiva-selective itch sensory fibers provides promising and unique neural targets for the development of new therapeutic strategies for antiocular itch. We provide proof of concept that silencing conjunctival itch-sensing fibers effectively alleviates ocular itch. This new therapeutic strategy is conceptually specific and is likely safe for the following reasons.

First, pharmacological silencing of conjunctival itch-sensing fibers exhibits a more sustained anti-itch effect than antihistamines currently used to treat ocular itch. In contrast to the binding of antihistamines to histamine receptors at the cell surface, the entry of QX-314 into conjunctival sensory fibers prevents the compound from being washed off by tear fluid and leads to sustained itch relief. Furthermore, silencing itch-sensing fibers reduces mast cell migration and accumulation at the allergen-challenged site and hence would decrease the amount of itch mediators released by mast cells, resulting in a less severe itch. This neuro-immune interaction offers a new explanation for the vicious cycle of itching and inflammation. Second, selective silencing of a highly restricted population of itch-sensing afferent fibers in the conjunctiva circumvents common side effects, including dry eye, glaucoma, cataract and ocular infections, caused by antihistamines or immunosuppressive corticosteroids and cyclosporine. Finally, this strategy would not affect the function of other conjunctival sensory fibers or corneal sensory fibers, which regulate basal tearing and protect the integrity of ocular surface from potential injuries<sup>49,50</sup>.

To develop new therapeutic strategies for allergic itch in humans, it is important to translate our discoveries from mice to humans. Despite the large size of the Mrgpr family in mice, there are only seven Mrgprs in humans. Interestingly, hMrgprX1 is sensitive to chloroquine and the peptide BAM8-22, both of which elicit histamine-independent itch in humans<sup>25,28,51</sup>. Our finding of selective projection of hMrgprX1-expressing sensory fibers to the conjunctiva, but not the cornea, in humans substantiates the pathogenic role of this population of neurons in ocular itch. Using *MRGPRX1*; *Mrgpr-clusterΔ<sup>-/-</sup>* mice, we confirmed the feasibility of pharmacological silencing of hMrgprX1<sup>+</sup> sensory fibers using QX-314 for treating allergic ocular itch. Furthermore, we found that hMrgprX1 functions as a principal itch receptor in ocular allergy, suggesting that hMrgprX1 itself is a promising anti-itch drug target in addition to being a useful molecular marker for itch afferent fibers in the conjunctiva. It will be important to develop potent and specific antagonists of hMrgprX1 for itch management in the future. The humanized mouse model *MRGPRX1*; *Mrgpr-clusterΔ<sup>-/-</sup>* will facilitate pharmacological study of the anti-itch effects of hMrgprX1 antagonists in vivo and help yield key pre-clinical evidence.

## Methods

Methods, including statements of data availability and any associated accession codes and references, are available at <https://doi.org/10.1038/s41591-018-0083-x>.

Received: 14 July 2016; Accepted: 2 May 2018;  
Published online: 9 July 2018

## References

- Ciprandi, G., Buscaglia, S., Cerqueti, P. M. & Canonica, G. W. Drug treatment of allergic conjunctivitis. A review of the evidence. *Drugs* **43**, 154–176 (1992).
- Abelson, M. B., Smith, L. & Chapin, M. Ocular allergic disease: mechanisms, disease sub-types, treatment. *Ocul. Surf.* **1**, 127–149 (2003).
- Wong, A. H., Barg, S. S. & Leung, A. K. Seasonal and perennial allergic conjunctivitis. *Recent Pat. Inflamm. Allergy Drug Discov.* **3**, 118–127 (2009).
- Ono, S. J. & Abelson, M. B. Allergic conjunctivitis: update on pathophysiology and prospects for future treatment. *J. Allergy Clin. Immunol.* **115**, 118–122 (2005).
- Yeniad, B., Alparlan, N. & Akarçay, K. Eye rubbing as an apparent cause of recurrent keratoconus. *Cornea* **28**, 477–479 (2009).
- Nagaki, Y., Hayasaka, S. & Kadoi, C. Cataract progression in patients with atopic dermatitis. *J. Cataract Refract. Surg.* **25**, 96–99 (1999).
- Ambati, B. K. et al. Corneal avascularity is due to soluble VEGF receptor-1. *Nature* **443**, 993–997 (2006).
- Cursiefen, C. Immune privilege and angiogenic privilege of the cornea. *Chem. Immunol. Allergy* **92**, 50–57 (2007).
- Paus, R., Schmelz, M., Bíró, T. & Steinhoff, M. Frontiers in pruritus research: scratching the brain for more effective itch therapy. *J. Clin. Invest.* **116**, 1174–1186 (2006).
- Oetjen, L. K. et al. Sensory neurons co-opt classical immune signaling pathways to mediate chronic itch. *Cell* **171**, 217–228.e13 (2017).
- Bonini, S. et al. Conjunctival provocation test as a model for the study of allergy and inflammation in humans. *Int. Arch. Allergy Appl. Immunol.* **88**, 144–148 (1989).
- Leonardi, A. The central role of conjunctival mast cells in the pathogenesis of ocular allergy. *Curr. Allergy Asthma Rep.* **2**, 325–331 (2002).
- Belmonte, C., Acosta, M. C., Schmelz, M. & Gallar, J. Measurement of corneal sensitivity to mechanical and chemical stimulation with a CO<sub>2</sub> esthesiometer. *Invest. Ophthalmol. Vis. Sci.* **40**, 513–519 (1999).
- Müller, L. J., Marfurt, C. F., Kruse, F. & Tervo, T. M. Corneal nerves: structure, contents and function. *Exp. Eye Res.* **76**, 521–542 (2003).
- Tanelian, D. L. & Beuerman, R. W. Responses of rabbit corneal nociceptors to mechanical and thermal stimulation. *Exp. Neurol.* **84**, 165–178 (1984).
- MacIver, M. B. & Tanelian, D. L. Structural and functional specialization of A delta and C fiber free nerve endings innervating rabbit corneal epithelium. *J. Neurosci.* **13**, 4511–4524 (1993).
- Beuerman, R. W. & Tanelian, D. L. Corneal pain evoked by thermal stimulation. *Pain* **7**, 1–14 (1979).
- Huang, C. C. et al. A histamine-independent itch pathway is required for allergic ocular itch. *J. Allergy Clin. Immunol.* **137**, 1267–1270.e6 (2016).
- Bautista, D. M. et al. TRPA1 mediates the inflammatory actions of environmental irritants and proalgesic agents. *Cell* **124**, 1269–1282 (2006).
- Wilson, S. R. et al. TRPA1 is required for histamine-independent, Mas-related G protein-coupled receptor-mediated itch. *Nat. Neurosci.* **14**, 595–602 (2011).
- Usoskin, D. et al. Unbiased classification of sensory neuron types by large-scale single-cell RNA sequencing. *Nat. Neurosci.* **18**, 145–153 (2015).
- Cavanaugh, D. J. et al. Distinct subsets of unmyelinated primary sensory fibers mediate behavioral responses to noxious thermal and mechanical stimuli. *Proc. Natl Acad. Sci. USA* **106**, 9075–9080 (2009).
- Kremer, A. E. et al. Lysophosphatidic acid is a potential mediator of cholestatic pruritus. *Gastroenterology* **139**, 1008–1018.e1 (2010).
- Liu, Q. et al. Mechanisms of itch evoked by β-alanine. *J. Neurosci.* **32**, 14532–14537 (2012).
- Liu, Q. et al. Sensory neuron-specific GPCR Mrgprs are itch receptors mediating chloroquine-induced pruritus. *Cell* **139**, 1353–1365 (2009).
- Han, L. et al. A subpopulation of nociceptors specifically linked to itch. *Nat. Neurosci.* **16**, 174–182 (2013).
- Liu, Q. et al. The distinct roles of two GPCRs, MrgprC11 and PAR2, in itch and hyperalgesia. *Sci. Signal.* **4**, ra45 (2011).
- Sikand, P., Dong, X. & LaMotte, R. H. BAM8-22 peptide produces itch and nociceptive sensations in humans independent of histamine release. *J. Neurosci.* **31**, 7563–7567 (2011).
- Reddy, V. B. et al. Redefining the concept of protease-activated receptors: cathepsin S evokes itch via activation of Mrgprs. *Nat. Commun.* **6**, 7864 (2015).
- Stantcheva, K. K. et al. A subpopulation of itch-sensing neurons marked by Ret and somatostatin expression. *EMBO Rep.* **17**, 585–600 (2016).
- Seal, R. P. et al. Injury-induced mechanical hypersensitivity requires C-low threshold mechanoreceptors. *Nature* **462**, 651–655 (2009).
- Lou, S., Duan, B., Vong, L., Lowell, B. B. & Ma, Q. Runx1 controls terminal morphology and mechanosensitivity of VGLUT3-expressing C-mechanoreceptors. *J. Neurosci.* **33**, 870–882 (2013).
- Zylka, M. J., Rice, F. L. & Anderson, D. J. Topographically distinct epidermal nociceptive circuits revealed by axonal tracers targeted to Mrgprd. *Neuron* **45**, 17–25 (2005).

34. Knop, E., Korb, D. R., Blackie, C. A. & Knop, N. The lid margin is an underestimated structure for preservation of ocular surface health and development of dry eye disease. *Dev. Ophthalmol.* **45**, 108–122 (2010).
35. Cevikbas, F. et al. A sensory neuron-expressed IL-31 receptor mediates T helper cell-dependent itch: involvement of TRPV1 and TRPA1. *J. Allergy Clin. Immunol.* **133**, 448–460 (2014).
36. Lee, M. G. et al. Agonists of the MAS-related gene (Mrgs) orphan receptors as novel mediators of mast cell-sensory nerve interactions. *J. Immunol.* **180**, 2251–2255 (2008).
37. Morita, T. et al. HTR7 mediates serotonergic acute and chronic itch. *Neuron* **87**, 124–138 (2015).
38. Kim, Y. S. et al. Central terminal sensitization of TRPV1 by descending serotonergic facilitation modulates chronic pain. *Neuron* **81**, 873–887 (2014).
39. Otsuki, J. A., Grassick, R., Seymour, D. & Kind, L. S. The use of 3H serotonin release from mast cells of the mouse as an assay for mediator liberation. *Immunol. Commun.* **5**, 27–39 (1976).
40. Razin, E. et al. IgE-mediated release of leukotriene C<sub>4</sub>, chondroitin sulfate E proteoglycan,  $\beta$ -hexosaminidase, and histamine from cultured bone marrow-derived mouse mast cells. *J. Exp. Med.* **157**, 189–201 (1983).
41. Panneton, W. M., Hsu, H. & Gan, Q. Distinct central representations for sensory fibers innervating either the conjunctiva or cornea of the rat. *Exp. Eye Res.* **90**, 388–396 (2010).
42. Zhao, Z. Q. et al. Cross-inhibition of NMBR and GRPR signaling maintains normal histaminergic itch transmission. *J. Neurosci.* **34**, 12402–12414 (2014).
43. Fleming, M. S. et al. The majority of dorsal spinal cord gastrin releasing peptide is synthesized locally whereas neuromedin B is highly expressed in pain- and itch-sensing somatosensory neurons. *Mol. Pain* **8**, 52 (2012).
44. Mishra, S. K., Holzman, S. & Hoon, M. A. A nociceptive signaling role for neuromedin B. *J. Neurosci.* **32**, 8686–8695 (2012).
45. Binshtok, A. M., Bean, B. P. & Woolf, C. J. Inhibition of nociceptors by TRPV1-mediated entry of impermeant sodium channel blockers. *Nature* **449**, 607–610 (2007).
46. Roberson, D. P. et al. Activity-dependent silencing reveals functionally distinct itch-generating sensory neurons. *Nat. Neurosci.* **16**, 910–918 (2013).
47. McNeil, B. D. et al. Identification of a mast-cell-specific receptor crucial for pseudo-allergic drug reactions. *Nature* **519**, 237–241 (2015).
48. Mousli, M. et al. Activation of rat peritoneal mast cells by substance P and mastoparan. *J. Pharmacol. Exp. Ther.* **250**, 329–335 (1989).
49. Parra, A. et al. Ocular surface wetness is regulated by TRPM8-dependent cold thermoreceptors of the cornea. *Nat. Med.* **16**, 1396–1399 (2010).
50. Belmonte, C., Aracil, A., Acosta, M. C., Luna, C. & Gallar, J. Nerves and sensations from the eye surface. *Ocul. Surf.* **2**, 248–253 (2004).
51. Abila, B., Ezeamuzie, I. C., Igbigbi, P. S., Ambakederemo, A. W. & Asomugha, L. Effects of two antihistamines on chloroquine and histamine induced weal and flare in healthy African volunteers. *Afr. J. Med. Med. Sci.* **23**, 139–142 (1994).

## Acknowledgements

We are grateful to M. W. Panneton, H. Hu, B. Kim, Z. F. Chen, T. P. Margolis and X. Dong for insightful discussions and comments on the manuscript, and we thank A. S. Yoo and Y. Liu for technical support. *Mrgpra3<sup>GFP-cre</sup>*, *Pir1<sup>GCaMP3/+</sup>* and *MRGPRX1;Mrgpr-cluster $\Delta^{-/-}$*  mice were generous gifts from X. Dong of Johns Hopkins University. *Mrgpr $\delta$ <sup>GFP/+</sup>* mice were from D. J. Anderson of the California Institute of Technology. *Trpm8<sup>GFP/+</sup>* mice were from G. Story. *Nav1.8<sup>cre</sup>*, *Nmb<sup>-/-</sup>*, *Nmbr<sup>-/-</sup>* and *Nmbr<sup>GFP</sup>* transgenic mice were from Z. -F. Chen of Washington University in St. Louis. *Slc17a8<sup>Cre/+</sup>* tissues were from Q. Ma of Dana-Farber Cancer Institute. This work was supported by the “Research to Prevent Blindness” (RPB) unrestricted grant to the Department of Ophthalmology (A.J.W.H. and Q.L.), and the National Institutes of Health (R01EY024704 and 1R01A1125743; Q.L.) and the Pew Scholar Award (Q.L.).

## Author contributions

C.-C.H. performed genetic axonal tracing, pharmacological and behavioral assays, calcium imaging experiments, immunofluorescence staining and data analysis and participated in manuscript preparation. W.Y. conducted retrograde tracing of ocular afferent neurons and single-cell picking, pharmacological and behavioral assays, calcium imaging, immunofluorescence and H&E staining and data analysis and participated in manuscript preparation. C.G. conducted single-cell qRT-PCR and immunofluorescence staining and assisted with mouse breeding strategy design, genetic ablation tests and manuscript preparation. H.J. performed electrophysiological recordings and data analysis. F.L. conducted TRPM8-GFP axonal tracing and ocular pain tests. M.X., in collaboration with W.Y., examined itch-sensing afferent fibers in human conjunctiva. S.D. performed the electrophysiological recordings and data analysis. G.Y. conducted calcium imaging of culture DRG neurons. B.D. and T.H. perfused *Slc17a8<sup>Cre/+</sup>*; *Rosa26<sup>tdTomato/+</sup>* mice and provided tissues for imaging. A.J.W.H. provided human tissues and contributed to experimental design and manuscript preparation. Q.L. planned and directed all of the experiments and wrote the paper.

## Competing interests

The authors declare no competing interests.

## Additional information

**Supplementary information** is available for this paper at <https://doi.org/10.1038/s41591-018-0083-x>.

**Reprints and permissions information** is available at [www.nature.com/reprints](http://www.nature.com/reprints).

**Correspondence and requests for materials** should be addressed to Q.L.

**Publisher's note:** Springer Nature remains neutral with regard to jurisdictional claims in published maps and institutional affiliations.

## Methods

**Animals.** C57BL/6J wild-type (stock no. 000664), B6;129S6-*Gt(Rosa)*26Sor<sup>tm1.4(CAG-tdTomato)Hze/J</sup> (*Rosa26*<sup>tdTomato</sup>; stock no. 007908), C57BL/6-*Gt(Rosa)26Sor<sup>tm1(HBEGF)Awai/J</sup>* (*Rosa26*<sup>HBEGF</sup>; stock no. 007900), B6N.Cg-*Sst<sup>tm2.1(crc)Zjh/J</sup>* (stock no. 018973) and B6N(Cg)-*Nmb<sup>tm1.1(KOMP)Vlgl/J</sup>* mice (stock no. 025862) were ordered from the Jackson Laboratory (Bar Harbor, ME). *Mrgpra3*<sup>GFP-cre</sup>, *Pirt*<sup>GCaMP3/+</sup> and *MRGPRX1;Mrgpr-clusterΔ<sup>-/-</sup>* mice were generous gifts from X. Dong of Johns Hopkins University. *Mrgpra3*<sup>GFP/+</sup> mice were from D. J. Anderson of the California Institute of Technology. *Trpm8*<sup>GFP/+</sup> mice were from G. Story. *Nav1.8*<sup>Cxcr</sup>, *Nmb*<sup>-/-</sup>, *Nmbr*<sup>-/-</sup> and *Nmbr*<sup>GFP</sup> transgenic mice were from Z. -F. Chen of Washington University in St. Louis. *Slc17a8*<sup>cre/+</sup> tissues were from Q. Ma of Dana-Farber Cancer Institute. Animals used for behavioral tests were backcrossed to the C57BL/6J background for at least ten generations and maintained in the congenic background. Male mice (two to three months old) were used for behavioral tests. All animal experiments were performed under protocols approved by Institutional Animal Care and Use Committee of Washington University School of Medicine.

**Reagents.** Chloroquine (C6628), histamine (H7250), β-alanine (A9920), serotonin (H9523), QX-314 (L5783), ovalbumin (A5503), DMEM/F12 (D6421), normal goat serum (G9023) and paraformaldehyde (P6148) were all purchased from Sigma-Aldrich (St. Louis, MO). Type I collagenase (17100017), dispase (17105051), anti-GFP antibody (A11122, lot no. 1925070; used at 1:1,000 dilution), and Alexa Fluor 488-conjugated goat anti-rabbit antibody (A11008, lot no. 1797971; used at 1:1,000 dilution), FITC-conjugated avidin (434411, lot no. 1561410A; used at 1:1,000 dilution), rhodamine-conjugated avidin (A003-00, lot no. 2496; used at 1:400 dilution), DiI (C7000), Alexa Fluor 488-conjugated WGA (W11261), Alexa Fluor 555-conjugated WGA-555 (W32464) and Imject Alum Adjuvant (PI77161) were purchased from Thermo Scientific (Asheville, NC). Leukotriene D<sub>4</sub> (20310) was purchased from Cayman Chemical (Ann Arbor, MI). IL-31 (200-31) was purchased from PeproTech (Rocky Hill, NJ). Chicken anti-GFP (GFP-1020, lot no. GFP697986; used at 1:1,000 dilution) was purchased from Aves Lab (Tigard, Oregon). Anti-DTR antibody (AF259NA, lot no. PX0911111; used at 1:200 dilution) was purchased from R&D Systems (Minneapolis, MN)<sup>32</sup>. anti-CGRP antibody (6009N T-4239, lot no.040269-6; used at 1:1,000 dilution) was purchased from Peninsula Laboratories International, Inc. (San Carlos, CA)<sup>26,52,53</sup>. X-gal staining kit (A10300K) was purchased from Genlantis (San Diego, CA). Anti-MrgprX1 antibody (used at 1:1,000 dilution) was generated by L. Han and X. Dong at the Johns Hopkins School of Medicine (Baltimore, MD). Cy5-conjugated donkey anti-goat antibody (705175147, lot no. 131485; used at 1:500 dilution) was purchased from Jackson ImmunoResearch Laboratories, Inc. (West Grove, PA). Optimum cutting temperature (OCT) embedding compound (4583) was purchased from Sakura Finetek USA, Inc. (Torrance, CA). Diphtheria Toxin (150) was purchased from List Biological Laboratories, Inc. (Campbell, CA).

**Histology.** Discarded cadaveric human donor corneal rims containing peripheral cornea, limbus and perilimbal conjunctiva from healthy donors were obtained from A.J.W.H. after corneal transplantation. The use of human tissue in this research conformed to the provisions of the Declaration of Helsinki and was exempted by the Washington University Human Subjects Protection Office. Medical and ocular histories of the donor had been de-identified and reviewed to ensure no evident ocular or systemic diseases. The procurement of donor corneas was performed under a standard protocol by the eye bank of Mid-America Transplants (St. Louis, MO).

All mice used for histology were anesthetized with ketamine-xylazine cocktail and transcardially perfused with ice-cold PBS followed by ice-cold 4% paraformaldehyde (PFA). Whole-mount corneal, oral mucosal, rectal, vaginal, conjunctiva, skin, and DRG tissues were dissected and imaged immediately using Nikon Ti-E microscope. Tissues used for frozen section were post-fixed in ice-cold PFA (4%, 0.5 h for the conjunctiva; 2%, 2 h for the skin; 3 h for the brain and 4%, 20 min for DRGs) and cryoprotected in 30% (wt/vol) sucrose-PBS solution for 24 h before they were embedded and frozen in OCT compound.

Tissues were sectioned at 20 μm using a Leica CM-1950 cryostat, allowed to air dry for 1 h and washed using PBS containing 0.1% Triton-X 100 (PBST). Tissue sections carrying endogenous fluorescence were directly mounted using Fluoromount-G. Tissue sections that required staining were blocked using 10% normal goat serum for 1 h at room temperature and incubated in primary antibody at 4 °C overnight followed by secondary antibody at room temperature for 2 h. X-gal staining was performed according to the manufacturer's instructions. For mast cell staining, tissue sections were incubated with FITC or rhodamine-conjugated avidin for 15 min at room temperature. After staining, tissue sections were mounted using Fluoromount-G and imaged after drying.

**Retrograde labeling.** WGA (1–2 μL) was injected into the stroma of the cornea or the submucosa of the palpebral conjunctiva of anesthetized mice using pulled glass micropipettes. Animals were euthanized for tissue collection 48–60 h after the injections.

DiI (1,1'-diiodo-3,3',3'-tetramethylindocarbocyanine perchlorate) retrograde neuronal labeling was performed as previously described<sup>18</sup>. In short, ~0.5 μL of 30 ng/μL DiI were injected into the palpebral conjunctiva of both lower

eyelids of anesthetized mice using a glass micropipette. Animals were used for histology 5 d after DiI injection.

**Cell picking.** WGA-labeled trigeminal neurons were collected from adult mice (6–8 week old, both males and females) and pooled into DMEM-F12 medium supplemented with 10% FBS and antibiotics (DH10). Afterwards, DRGs were digested using a collagenase-dispase solution at 32 °C for 20 min, triturated, pelleted and resuspended in 400 μL of DH10 medium per mouse. 200 μL of the cell suspension was then carefully pipetted on top of 1.2 mL of freshly prepared 15% BSA in a 1.5-mL microcentrifuge tube and centrifuged at 400 g for 4 min to separate neurons from myelin and debris. After purification, the BSA supernatant was aspirated, and the pelleted neurons were resuspended in DH10 media. All steps after digestion were performed on ice.

Cells were isolated manually using a controlled cell-picking setup, constructed in-house around a Leica DMi6000 inverted epifluorescent microscope (Buffalo Grove, IL) and a Narishige MMO-202ND micromanipulator (Amityville, NY). WGA-labeled neurons were captured into pulled glass micropipettes with 20-μm-wide openings and ejected into PCR tubes containing 10 μL of lysis buffer and RNase inhibitor.

**Real-time qRT-PCR.** cDNA libraries from single neurons were generated using Invitrogen SuperScript III CellsDirect cDNA Synthesis Kit (ThermoFisher, 18080300) and as previously described<sup>25</sup>. In short, manually isolated neurons were collected into 0.2-mL thin-walled PCR tubes pre-filled with 10 μL supplied lysis buffer and RNase inhibitor, flash frozen on dry ice and stored at –80 °C until cDNA synthesis. DNase digestion was performed for all cells. First-strand cDNA was generated using 100 nmols (50 mM, 2 μL) of oligo(dT)<sub>20</sub>. All other steps were performed according to the manufacturer's protocol.

qPCR was performed using power SYBR Green master mix (ABI 4368702) on an ABI StepOnePlus qPCR machine. Single-cell genomic DNA was used as the negative control and FACS-isolated DRG neurons (~36,000 neurons, diluted 1:36,000) were used as the positive control. *Gapdh* was used to identify and exclude samples without input or with failed cDNA synthesis. All primer sets were validated before use, and PCR products were selected for further sequence validation. All gene expression data is presented as folds of *Gapdh* expression, calculated using  $2^{-\Delta Ct(\text{target gene}) - \Delta Ct(\text{Gapdh})}$ .

**Behavioral assays.** All animal behavioral experiments were performed and analyzed in a blinded manner. Ocular itch experiments were performed as described previously<sup>18</sup>. In short, 2- to 3-month-old mice were manually restrained, and 2.5 μL of pruritogens were applied directly into the inferior conjunctival sac. Afterwards, animals were returned to recording chambers and filmed for 30 min. Scratch bouts directed at the treated conjunctiva were scored after completion of filming.

In the ocular cold pain tolerance assays, acclimated test animals were manually restrained, and a 0.5 L per min stream of temperature-controlled air was applied directly to the exposed corneas. Blinking, eye closure and other responses were quantified afterwards.

Mast cell-dependent allergy models were generated as described previously<sup>18</sup>. In short, mice were given two intraperitoneal (i.p.) injections of a 1:1 mixture of 0.01% (wt/vol) ovalbumin and Imject Alum 10 d apart to induce allergic sensitivity to OVA. Seven days after the second i.p. injection, sensitized animals were used for behavioral experiments and challenged with 250 μg of ovalbumin to induce allergic ocular itch. To pharmacologically silence itch-sensing fibers in the conjunctiva, 2 μL mixture solution (1% QX-314 + 4 mM chloroquine) was applied to the lower conjunctival sac of immunized mice before ovalbumin challenging. As a positive control, 0.4% pheniramine was used as a pretreatment to suppress histamine-dependent itch signaling in the conjunctiva. 10 min, 30 min, 1 h, 24 h or 48 h after pretreatments, mice were challenged with ovalbumin, video-recorded for 30 min and quantified blindly.

Mice used in the *Mrgpra3*<sup>+</sup> neuron ablation model were generated using a protocol adapted from previously published literature<sup>18</sup>. Two-month-old *Mrgpra3*<sup>gfp-cre+</sup>, *Rosa26*<sup>HBEGF/+</sup> mice and *Rosa26*<sup>HBEGF/+</sup> control littermates were given two i.p. injections of 30 μg per kg body weight diphtheria toxin (DTX) 3 d apart (*HBEGF* is the gene encoding diphtheria toxin receptor (DTR)). Treated animals were used for behavioral experiments 4 weeks after the second DTX injection.

**Calcium imaging.** Whole-mount calcium imaging of the conjunctiva was performed as described previously<sup>18</sup>. In short, conjunctivae were dissected and allowed to recover in oxygenated recording buffer at room temperature for 30 min. After recovery, dissected explants were imaged using a Nikon Ti-E inverted microscope and Photometrics CoolSnap HQ<sub>2</sub> CCD camera (Tucson, AZ). The responses of conjunctival sensory fibers to pruritogens were defined as changes in *GCaMP3* fluorescence intensity ( $\Delta F/F_0$ ) using the Nikon NIS Elements AR software.

Calcium imaging of cultured DRG neurons was performed as described previously<sup>25</sup>. DRGs were collected from euthanized mice, aged 3–4 weeks, and pooled in DMEM-F12 medium supplemented with 10% FBS and antibiotics (DH10). Afterwards, DRGs were digested using a collagenase-dispase solution at

37 °C for 30 min, triturated, pelleted, and resuspended in DH10 media. Afterwards, dissociated DRGs were seeded onto glass coverslips coated with poly-D-lysine and laminin, supplemented with 20 ng/mL nerve growth factor and 50 ng/mL glial cell-derived growth factor and cultured at 37 °C for 18–24 h before use.

**Electrophysiology.** Cultured sensory neurons expressing tdTomato fluorescence were viewed under an epifluorescent BX50 Olympus microscope. Cells were bathed at room temperature ( $22 \pm 2$  °C) in external solution containing (in mM): 145 NaCl, 3 KCl, 2.5 CaCl<sub>2</sub>, 1.2 MgCl<sub>2</sub>, 7 glucose, and 10 HEPES, adjusted to pH 7.4 with NaOH and 305 mOsm with sucrose. Borosilicate, filamented glass electrodes with 1.7–3.5 MΩ resistance contained (in mM): 130 K-gluconate, 5 KCl, 5 NaCl, 3 Mg-ATP, 0.3 EGTA, 10 HEPES, adjusted to pH 7.3 with KOH and 295 mOsm with sucrose. Pipette potential was zeroed before seal formation, cell capacitance was cancelled electronically and series resistance was compensated  $\geq 70\%$ . After gigaseal formation and break-in, chloroquine (200 μM) was bath-applied with 5 mM QX-314 in voltage-clamp mode followed by a series of voltage steps while evoked current was monitored. For sodium currents, neurons were held at  $-70$  mV, and 100-ms voltage steps were delivered, each increasing by 5 mV until +35 mV was reached. Data were collected with a HEKA EPC 10 amplifier (Heka Electronic, Lambrecht/Pfalz, Germany), digitized at 20 kHz and recorded on a PC running Patchmaster software (v2; Heka Electronic).

Whole-cell current-clamp recordings of TG neurons from *MRGPRX1*; *Mrgpr-clusterΔ<sup>-/-</sup>* mice were performed using a MultiClamp 700B amplifier and pCLAMP 10.5 software (Axon Instruments, US).

**Statistical analysis.** All histology, calcium imaging, and electrophysiology experiments were repeated using tissues from at least three different mice. All

attempts at replication were successful. Sample sizes for itch and pain behavior tests were selected on the basis of power analysis of related publications<sup>18,25,37</sup> and ‘sample size determination’<sup>38</sup> (more details in Nature Research Reporting Summary). Animals were placed into experimental groups on the basis of either their genotype (no randomization) or through simple randomization. Itch and pain behaviors were scored by researchers blinded to mouse genotypes or treatment condition. No animal or data point was excluded from analysis. All data are presented as mean  $\pm$  s.e.m. F test was used to evaluate whether the variance similar between the groups that are being statistically compared. Statistical significances were determined using two-tailed Student’s *t* test (for two groups) or one-way ANOVA (for three or more groups). Differences were considered significant at  $P \leq 0.05$ .

**Reporting Summary.** Further information on experimental design is available in the Nature Research Reporting Summary linked to this article.

**Data availability.** All data generated or analyzed during this study are included in this published article (and the accompanying Supplementary Information).

## References

- McCoy, E. S. et al. Peptidergic CGRP $\alpha$  primary sensory neurons encode heat and itch and tonically suppress sensitivity to cold. *Neuron* **78**, 138–151 (2013).
- Liu, Q. et al. Molecular genetic visualization of a rare subset of unmyelinated sensory neurons that may detect gentle touch. *Nat. Neurosci.* **10**, 946–948 (2007).
- Dell, R. B., Holleran, S. & Ramakrishnan, R. Sample size determination. *ILAR J.* **43**, 207–213 (2002).

## Reporting Summary

Nature Research wishes to improve the reproducibility of the work that we publish. This form provides structure for consistency and transparency in reporting. For further information on Nature Research policies, see [Authors & Referees](#) and the [Editorial Policy Checklist](#).

### Statistical parameters

When statistical analyses are reported, confirm that the following items are present in the relevant location (e.g. figure legend, table legend, main text, or Methods section).

n/a | Confirmed

- The exact sample size ( $n$ ) for each experimental group/condition, given as a discrete number and unit of measurement
- An indication of whether measurements were taken from distinct samples or whether the same sample was measured repeatedly
- The statistical test(s) used AND whether they are one- or two-sided  
*Only common tests should be described solely by name; describe more complex techniques in the Methods section.*
- A description of all covariates tested
- A description of any assumptions or corrections, such as tests of normality and adjustment for multiple comparisons
- A full description of the statistics including central tendency (e.g. means) or other basic estimates (e.g. regression coefficient) AND variation (e.g. standard deviation) or associated estimates of uncertainty (e.g. confidence intervals)
- For null hypothesis testing, the test statistic (e.g.  $F$ ,  $t$ ,  $r$ ) with confidence intervals, effect sizes, degrees of freedom and  $P$  value noted  
*Give  $P$  values as exact values whenever suitable.*
- For Bayesian analysis, information on the choice of priors and Markov chain Monte Carlo settings
- For hierarchical and complex designs, identification of the appropriate level for tests and full reporting of outcomes
- Estimates of effect sizes (e.g. Cohen's  $d$ , Pearson's  $r$ ), indicating how they were calculated
- Clearly defined error bars  
*State explicitly what error bars represent (e.g. SD, SE, CI)*

*Our web collection on [statistics for biologists](#) may be useful.*

### Software and code

Policy information about [availability of computer code](#)

Data collection

Nikon NIS Elements AR software for calcium imaging data collection  
pCLAMP 10.5 software (Axon Instruments, U.S.) and Patchmaster software (v2; Heka Electronic) for electrophysiology data collection

Data analysis

Nikon NIS Elements AR software for calcium imaging data analysis  
pCLAMP 10.5 software (Axon Instruments, U.S.) and Patchmaster software (v2; Heka Electronic) for electrophysiology data analysis  
GraphPad Prism5 for statistical analysis

For manuscripts utilizing custom algorithms or software that are central to the research but not yet described in published literature, software must be made available to editors/reviewers upon request. We strongly encourage code deposition in a community repository (e.g. GitHub). See the Nature Research [guidelines for submitting code & software](#) for further information.

### Data

Policy information about [availability of data](#)

All manuscripts must include a [data availability statement](#). This statement should provide the following information, where applicable:

- Accession codes, unique identifiers, or web links for publicly available datasets
- A list of figures that have associated raw data
- A description of any restrictions on data availability

All data generated or analysed during this study are included in this published article (and its supplementary information files).

## Field-specific reporting

Please select the best fit for your research. If you are not sure, read the appropriate sections before making your selection.

Life sciences  Behavioural & social sciences

For a reference copy of the document with all sections, see [nature.com/authors/policies/ReportingSummary-flat.pdf](https://www.nature.com/authors/policies/ReportingSummary-flat.pdf)

## Life sciences

### Study design

All studies must disclose on these points even when the disclosure is negative.

Sample size	The criteria for determining the number of animals used in itch and pain behavioral assays is based on the "Sample size determination" (Dell et al. 2002, ILAR J, 43(4), 207–13), and analysis of recently published papers that are relevant to our study (reference 56-58 for online method). Three factors are important to calculate sample size (Dell et al, 2002). 1. the size of the effect under study (difference between experimental groups) 2. the desired power of the experiment to detect the effect (usually 80-90%) 3. the significance level (we chose 0.05). The animals used in our current study were all age-matched, congenic C57BL/6 inbred male mice. Animals with the same genotype are genetically identical, while the only genetic differences between genotypes are at the indicated alleles. Furthermore, all practically feasible care was observed by our researchers and animal care technicians to ensure that these mice received identical upbringing until our experiment. Hence, individual variation between animals with the same genotype is minimal. For statistical comparison of two genotypes, there is much less variability in the results and our sample sizes are sufficient.
Data exclusions	No animal or data point was excluded from analysis
Replication	All histology, calcium imaging, and electrophysiology experiments were repeated using tissues from at least 3 different mice. All attempts at replication were successful.
Randomization	Animals were placed into experimental groups based either on their genotype (no randomization) or through simple randomization.
Blinding	Itch and pain behaviors were scored by researchers blinded to mouse genotypes or treatment condition.

## Materials & experimental systems

Policy information about [availability of materials](#)

n/a	Involvement in the study
<input checked="" type="checkbox"/>	<input type="checkbox"/> Unique materials
<input type="checkbox"/>	<input checked="" type="checkbox"/> Antibodies
<input type="checkbox"/>	<input checked="" type="checkbox"/> Eukaryotic cell lines
<input type="checkbox"/>	<input checked="" type="checkbox"/> Research animals
<input checked="" type="checkbox"/>	<input type="checkbox"/> Human research participants

### Antibodies

Antibodies used

Anti-GFP antibody (A11122, Lot#1925070; used at 1:1000 dilution), and Alexa Fluor® 488-conjugated goat anti-rabbit antibody (A11008, Lot#1797971; used at 1:1000 dilution), FITC-conjugated avidin (434411, Lot#1561410A; used at 1:1000 dilution), and Rhodamine-conjugated avidin (A003-00, Lot#2496; used at 1:400 dilution) were purchased from Thermo Scientific (Asheville, NC). Chicken anti-GFP (GFP-1020, Lot#GFP697986; used at 1:1000 dilution) was purchased from Aves Lab (Tigard, Oregon). Anti-DTR antibody (AF259NA, Lot#PX0911111; used at 1:200 dilution) was purchased from R&D Systems (Minneapolis, MN). Anti-CGRP antibody (T-4239, Lot#040269-6; used at 1:1000 dilution) was purchased from Peninsula Laboratories International, Inc. (San Carlos, CA). Anti-hMrgprX1 antibody (used at 1:1000 dilution) was generated by Liang Han in Dr. Xinzhong Dong's lab at the Johns Hopkins School of Medicine in Baltimore, MO. Cy5-conjugated donkey anti-goat antibody (705175147, Lot#131485; used at 1:500 dilution) was purchased from Jackson ImmunoResearch Laboratories, Inc. (West Grove, PA).

## Validation

Anti-MrgprX1 antibody was validated in this study using humanized hMrgprX1 transgenic mice in which human MrgprX1 replaced mouse Mrgprs in primary sensory neurons. Validation data for other antibodies are available from the commercial providers.

## Eukaryotic cell lines

Policy information about [cell lines](#)

## Cell line source(s)

KNRK cells obtained from ATCC

## Authentication

The authentication data are available from ATCC

## Mycoplasma contamination

The cell line was not tested for mycoplasma contamination in the authors' laboratory.

Commonly misidentified lines  
(See [ICLAC](#) register)

No commonly misidentified cell lines were used

## Research animals

Policy information about [studies involving animals](#); [ARRIVE guidelines](#) recommended for reporting animal research

## Animals/animal-derived materials

C57BL/6J wild-type (Stock#: 000664), B6;129S6-Gt(ROSA)26Sortm14(CAG-tdTomato)Hze/J (ROSA26tdTomato; Stock#:007908), C57BL/6-Gt(ROSA)26Sortm1(HBEGF)Awai/J (ROSA26DTR; Stock#:007900), B6N.Cg-Ssttm2.1(cre)Zjh/J (Stock#: 018973) and B6N(Cg)-Nmbtm1.1(KOMP)Vlcr/J mice (025862) were ordered from the Jackson Laboratory (Bar Harbor, ME). MrgprA3EGFP-Cre, PirtGCaMP3/+ and hMrgprX1;Mrgpr-cluster -/- mice were generous gifts from Dr. Xingzhong Dong of Johns Hopkins University. MrgprDEGFP/+ mice were from Dr. David J. Anderson of the California Institute of Technology. TRPM8GFP/+ mice were from Dr. Gina Story. Nav1.8Cre, NMB-/-, NMBR-/-, and NMBReGFP transgenic mice were from Dr. Zhou-Feng Chen of Washington University in St. Louis. VGLUT3Cre/+ tissues were from Dr. Qiufu Ma of Dana-Farber Cancer Institute. Animals used for behavioral tests were backcrossed to the C57BL/6J background for at least 10 generations and maintained in the congenic background. Male mice (two to three months old) were used for behavioral tests. All animal experiments were performed under protocols approved by the Animal Care and Use Committee of Washington University School of Medicine.

## Method-specific reporting

n/a	Involvement in the study
<input checked="" type="checkbox"/>	<input type="checkbox"/> ChIP-seq
<input checked="" type="checkbox"/>	<input type="checkbox"/> Flow cytometry
<input checked="" type="checkbox"/>	<input type="checkbox"/> Magnetic resonance imaging

In the format provided by the authors and unedited.

# Anatomical and functional dichotomy of ocular itch and pain

Cheng-Chiu Huang<sup>1,7,9</sup>, Weishan Yang<sup>1,9</sup>, Changxiong Guo<sup>1</sup>, Haowu Jiang<sup>1</sup>, Fengxian Li<sup>1,2</sup>, Maolei Xiao<sup>1</sup>, Steve Davidson<sup>3</sup>, Guang Yu<sup>4</sup>, Bo Duan<sup>5,8</sup>, Tianwen Huang<sup>5</sup>, Andrew J. W. Huang<sup>6</sup> and Qin Liu<sup>1,6\*</sup>

---

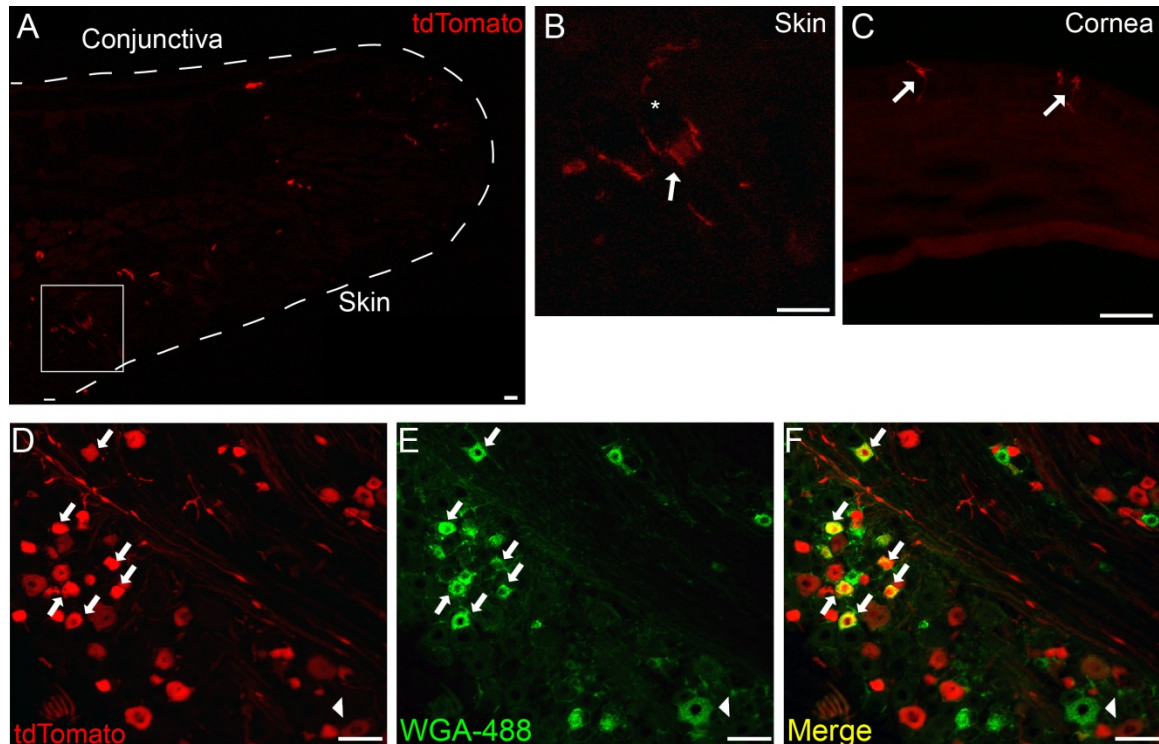
<sup>1</sup>Department of Anesthesiology and Center for the Study of Itch, Washington University School of Medicine, St. Louis, MO, USA. <sup>2</sup>Department of Anesthesiology, Zhujiang Hospital, Southern Medical University, Guangzhou, People's Republic of China. <sup>3</sup>Department of Anesthesiology and Pain Research Center, University of Cincinnati College of Medicine, Cincinnati, OH, USA. <sup>4</sup>School of Medicine and Life Sciences, Nanjing University of Chinese Medicine, Jiangsu, China. <sup>5</sup>Dana-Farber Cancer Institute and Department of Neurobiology, Harvard Medical School, Boston, MA, USA. <sup>6</sup>Department of Ophthalmology and Visual Sciences, Washington University School of Medicine, St. Louis, MO, USA. <sup>7</sup>Present address: Merck Research Laboratories, South San Francisco, CA, USA. <sup>8</sup>Present address: Department of Molecular, Cellular, and Developmental Biology, University of Michigan, Ann Arbor, MI, USA. <sup>9</sup>These authors contributed equally: Cheng-Chiu Huang, Weishan Yang. \*e-mail: [qinliu@wustl.edu](mailto:qinliu@wustl.edu)



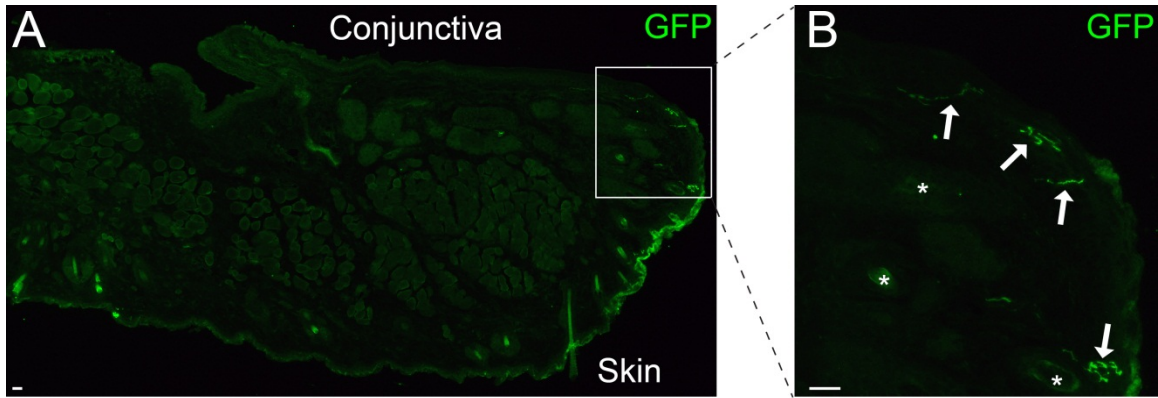
**Supplemental Table S2:** The axonal projection of various populations of primary sensory neurons to the conjunctiva, cornea and skin

Table 1: Mouse lines	Conjunctiva	Cornea	Back Skin
<i>Pirt</i> <sup>GCaMP3/+</sup>	+++++	+++++	+++++
<i>Nav1.8: Scn10a</i> <sup>cre/+</sup> ; <i>Rosa26</i> <sup>tdT/+</sup>	+++	+++++	++++
<i>Trpv1</i> <sup>ALPP/+</sup>	+++	++++	+++
<i>Trpm8</i> <sup>gfp/+</sup>	+	++++	++
<i>Mrgprd</i> <sup>egfp/+</sup>	+	absent	+++
<i>Mrgpra3</i> <sup>cre/+</sup> ; <i>Rosa26</i> <sup>tdT/+</sup>	+++	absent	+++
<i>Sst</i> <sup>cre/+</sup> ; <i>Rosa26</i> <sup>tdT/+</sup>	absent	absent	+++
<i>Vglut3: Slc17a8</i> <sup>cre/+</sup> ; <i>Rosa26</i> <sup>tdT/+</sup>	absent	++	+++
CGRP (immunofluorescence)	+++	++++	+++

## Supplemental Figures



**Fig. S1:** Low-threshold mechanosensitive C fiber neurons that express vesicular glutamate transporter 3 (VGLUT3, gene *Slc17a8*) do not innervate the conjunctiva (A) *Slc17a8<sup>cre/+</sup>; Rosa26<sup>tdTomato/+</sup>* (*Slc17a8<sup>tdTomato/+</sup>*) sensory fibers in a section of an eyelid. (B) High magnification view of boxed area in (A). Asterisk indicates a hair follicle. Arrow indicates *Slc17a8<sup>tdTomato/+</sup>* sensory fibers (C) *Slc17a8<sup>tdTomato/+</sup>* sensory fibers in a section of cornea. Arrows indicate VGLUT3<sup>+</sup> sensory fibers. (D-F) WGA-mediated retrograde labeling of corneal afferent neurons in *Slc17a8<sup>tdTomato/+</sup>* mice. Arrows indicate co-localization of tdTomato<sup>+</sup> neurons (red) and WGA (green) in the section of trigeminal ganglion. Arrowhead indicates a large diameter neuron labelled only by WGA. Representative images shown were chosen from 3 trigeminal ganglia imaged from three mice. Scale bars: 50  $\mu$ m.



**Fig. S2:** Sparse innervation of TRPM8<sup>+</sup> sensory fibers in the conjunctiva (A) *Trpm8*<sup>gfp/+</sup> sensory fibers in a section of an eyelid. (B) High magnification view of boxed area in (A). Arrows indicate GFP<sup>+</sup> fibers. Asterisks indicate hair follicles in the eyelid skin. Representative images were chosen from 6 conjunctivae imaged from three mice. Scale bars: 50  $\mu$ m.

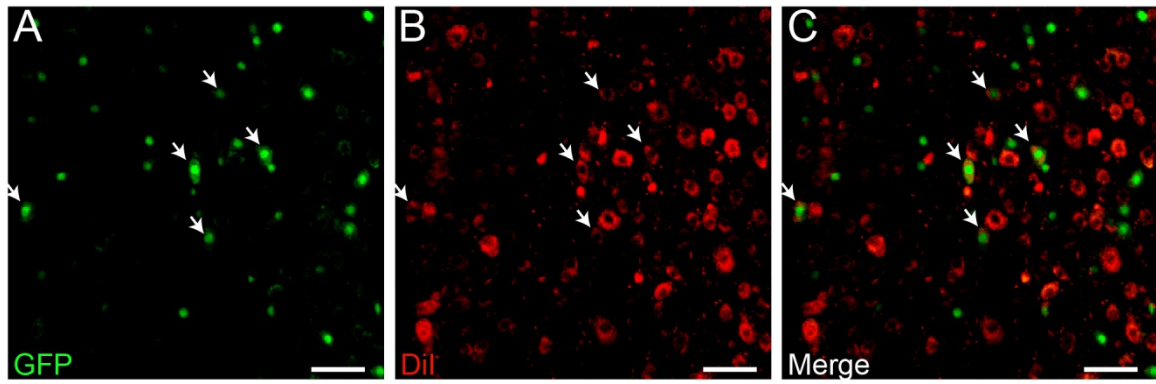


**Fig. S3:** A group of conjunctival afferent neurons express MrgprA3. **(A-C)** Dil-mediated retrograde labeling of conjunctival afferent neurons in *MrgprA3<sup>gfp-cre</sup>* mice. Arrows indicate co-localization of GFP<sup>+</sup> neurons (green) and Dil (red) in the section of trigeminal ganglion. Representative images shown were chosen from 3 trigeminal ganglia imaged from 3 mice. Scale bars: 50  $\mu$ m.

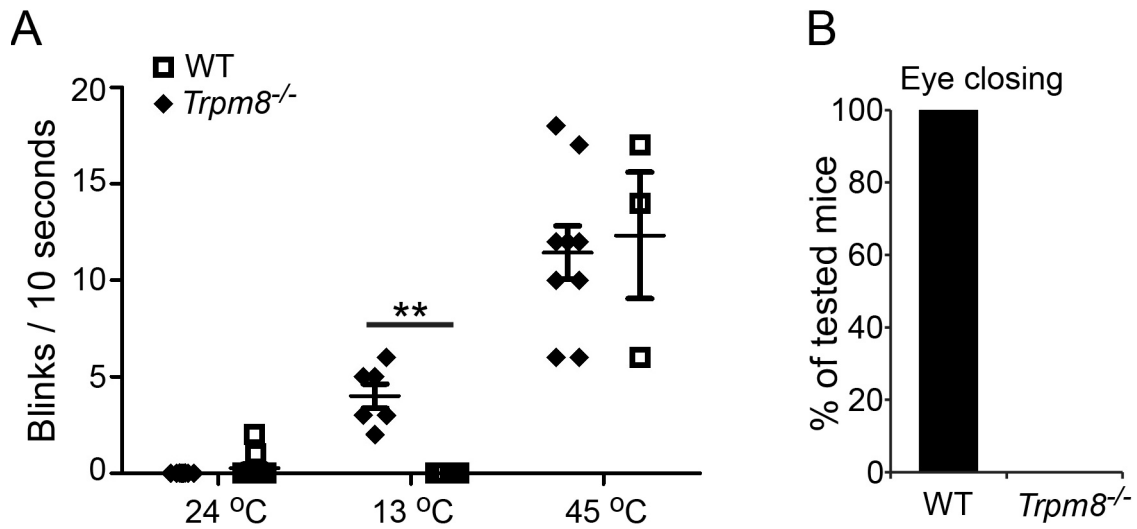


**Fig. S4:** TRPM8 mediates ocular pain induced by the cold temperature. **(A)** Blinking responses to air flow (0.5 L/min) at different temperatures in WT (n=11, 6, 9, respectively) and *Trpm8*<sup>-/-</sup> mice (n=11, 8, 3, respectively). Data are expressed as mean±s.e.m. Statistical analysis by two tailed Student's t-test (\*\*P=0.0015). **(B)** Eye-closing behavior to air flow (0.5 L/min) at different temperature in WT (n=6) and *Trpm8*<sup>-/-</sup> mice (n=3).

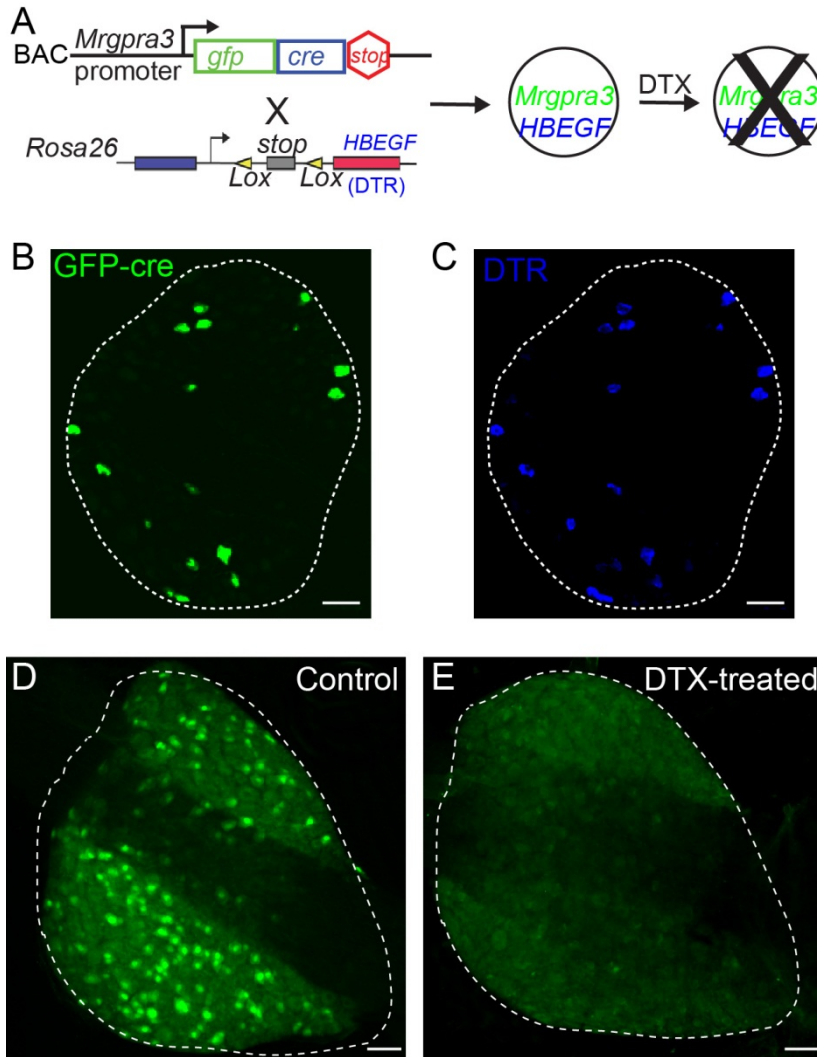


**Fig. S5:** Genetic- and temporal-specific ablation of MrgprA3<sup>+</sup> neurons. **(A)** Combining Cre-Lox and diphtheria toxin receptor (DTR, gene *HBEGF*) approaches to ablate MrgprA3<sup>+</sup> neurons. **(B-C)** All *Mrgpra3*<sup>gfp-cre</sup> neurons (green) express DTR (blue). No ectopic DTR expression was detected. **(D-E)** Stacked confocal microscopy images of the whole DRG from *Mrgpra3*<sup>gfp-cre</sup>; *Rosa*<sup>HBEGF/+</sup> mice before **(D)** and after **(E)** diphtheria toxin treatment. Representative images were chosen from DRGs imaged from 3 mice. Scale bars: 50  $\mu$ m.

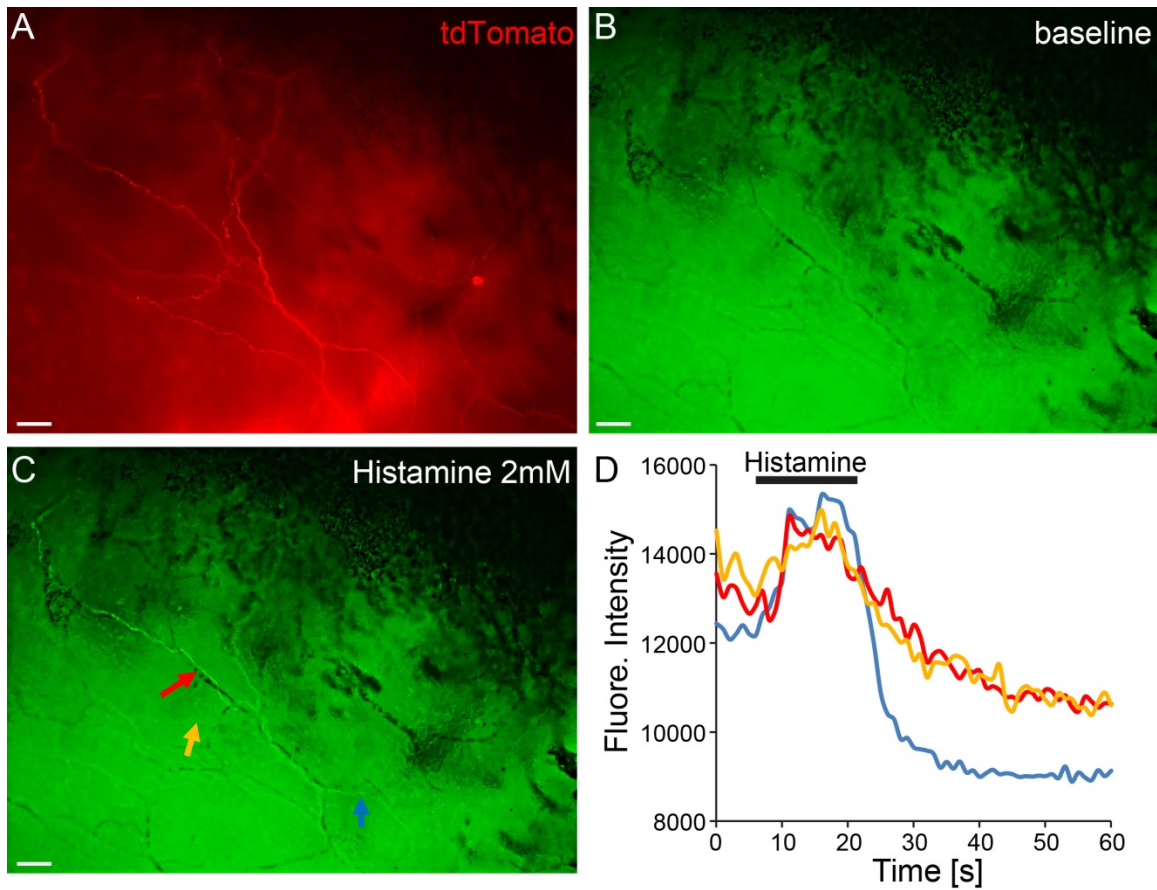


**Fig. S6:** MrgprA3<sup>+</sup> conjunctival fibers response to histamine. **(A)** *Mrgpra3*<sup>gfp-cre/+</sup>; *Rosa26*<sup>tdTomato/+</sup>; *Pirt*<sup>GCaMP3/+</sup> sensory fibers (red) in the conjunctiva. **(B)** Baseline of GCaMP3 fluorescence in the conjunctiva explant. **(C)** Increased GCaMP3 fluorescence upon 2 mM histamine stimulation. Arrows indicate activated MrgprA3<sup>+</sup> sensory fibers. **(D)** Dynamics of GCaMP3 fluorescence upon histamine stimulation in MrgprA3<sup>+</sup> sensory fibers from **(C)**. Representative images were chosen from 5 conjunctival explants imaged from 3 mice. Scale bars: 50  $\mu$ m.

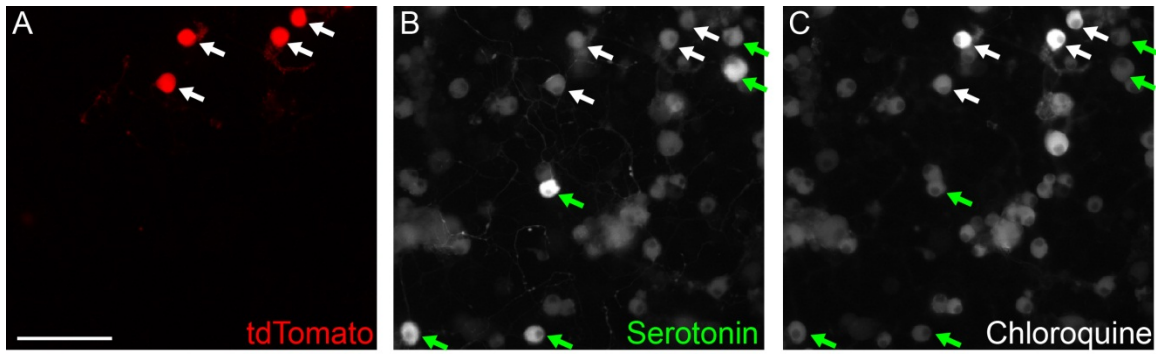


**Fig. S7:**  $MrgprA3^+$  DRG neurons respond to chloroquine but not serotonin. (A) DRG neurons cultured from  $Mrgpra3^{cre/+}$ ;  $Rosa26^{tdTomato/+}$ ;  $Pirt^{GCaMP3/+}$  mice. White arrows indicate  $MrgprA3^+$  DRG neurons. (B) Increased GCaMP3 fluorescence upon 10  $\mu$ M serotonin stimulation. (C) Increased GCaMP3 fluorescence upon 1 mM chloroquine stimulation. Green arrows indicate serotonin-sensitive neurons, which do not express  $MrgprA3$  and are insensitive to chloroquine. The experiment was repeated independently three times with similar results. Scale bars: 100  $\mu$ m.

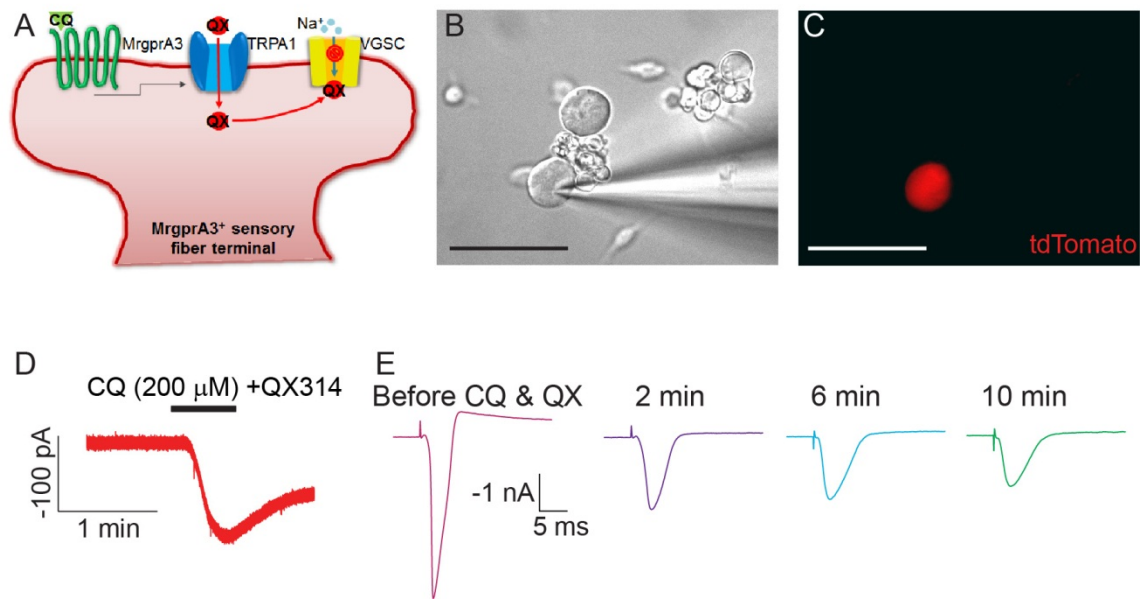


**Fig. S8:** Chloroquine-mediated entry of QX-314 decreases inward sodium current in MrgprA3<sup>+</sup> neurons. **(A)** Diagram depicting the action model of QX-314 in MrgprA3<sup>+</sup> neurons. **(B)** Representative photomicrograph of a recorded sensory neuron from *Mrgpra3<sup>gfp-cre/+</sup>; Rosa26<sup>tdTomato/+</sup>* (*Mrgpra3<sup>tdTomato/+</sup>*) mice. **(C)** The presence of tdTomato (red) indicates that the recorded neuron is MrgprA3<sup>+</sup>. Scale bars: 100 μm. **(D)** Inward currents triggered by application of chloroquine and QX-314 **(E)** Representative traces of inward sodium current recorded before and after application of CQ and QX-314.

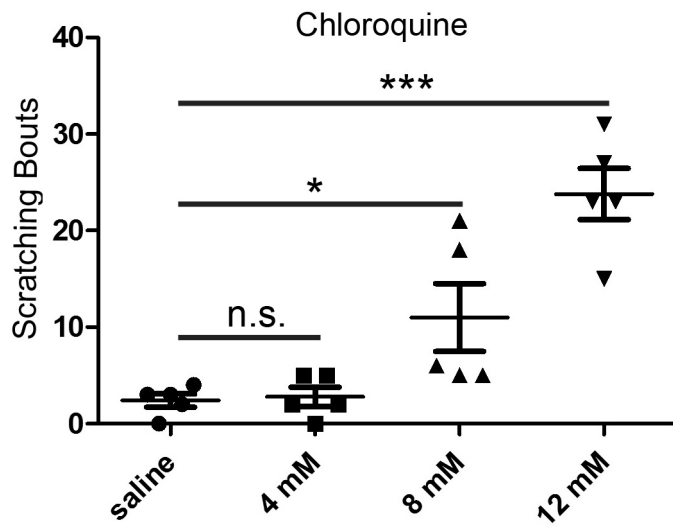


**Fig. S9:** Dose-dependent ocular scratching behavior evoked by topical chloroquine application in the conjunctiva sac of WT mice (n=5/group). All data are expressed as mean±s.e.m. Statistical analysis by two tailed Student's *t*-test (4 mM vs. saline, P=0.744; 8 mM vs. saline, \*P=0.04; 12 mM vs. saline, \*\*\*P=0.0009).

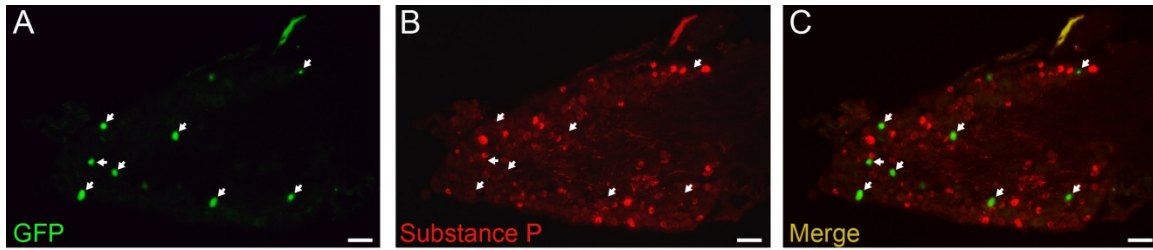


**Fig. S10:** MrgprA3<sup>+</sup> neurons do not express substance P. **(A)** DRG section of *Mrgpra3<sup>gfp-cre/+</sup>* mouse. **(B)** Immunofluorescence of substance P. **(C)** Merged image of **(A)** and **(B)**. Arrows indicate MrgprA3<sup>+</sup> DRG neurons, which do not overlap with substance P immunofluorescence signals. Representative images were chosen from DRGs imaged from 3 mice. Scale bars: 50  $\mu$ m.